Spring 2-2016

Implementation of Space-Time Finite Element Formulation in Elastodynamics

Sidharth Ramesh
Rose-Hulman Institute of Technology, rameshs1@rose-hulman.edu

Implementation of Space-Time Finite Element Formulation in Elastodynamics

A thesis

Submitted to the Faculty

Of

Rose-Hulman Institute of Technology

By

Sidharth Ramesh

In partial fulfilment of the requirements for the degree

Of

Masters of Science in Mechanical Engineering

February 2016

ROSE-HULMAN INSTITUTE OF TECHNOLOGY

Final Examination Report

Sidharth Ramesh — Name

Mechanical Engineering — Graduate Major

Thesis Title: Implementation of Space-Time Finite Element Formulation in Elastodynamics

DATE OF EXAM: January 21, 2016

EXAMINATION COMMITTEE:

	Thesis Advisory Committee	Department
Thesis Advisor:	Simon Jones	ME
	Lorraine Olson	ME
	Allen Holder	MA

PASSED X **FAILED** _____

Abstract

Ramesh, Sidharth

M.S.M.E

Rose-Hulman Institute of Technology

Feb 2016

Implementation of Space-Time Finite Element Formulation in Elastodynamics

Thesis Advisor: Dr. Simon Jones

Elastodynamics is an academic field that is involved in solving problems related to the field of wave propagation in continuous solid medium. Finite element methods have long been an accepted way of solving elastodynamics problems in the spatial dimension. Considerable thought has been given to ways of implementing finite element discretization in the temporal dimension as well. A particular method of finite element solving called space-time finite element formulation is explored in this thesis, which is a relatively recent technique for discretization in spatial and temporal dimensions. The present thesis explores the implementation of the Space-Time finite element formulation in solving classical elastodynamics examples, such as the mass-on-spring for a single degree of freedom and for an axially vibrating bar with multiple degrees of freedom. The space-time formulation is compared with existing finite difference techniques, such as the central difference method, for computational expenditure and accuracy. In the mass-on-spring case, the central difference method and linear time finite elements yield relatively similar results, whereas quadratic time finite elements are more accurate but take more time computationally. In the axially vibrating bar case, central difference is computationally more efficient than the Space-Time finite element method. The final section concludes our findings and critiques the numerical effectiveness of the space-time finite element formulation.

Dedication

To my Parents for wholeheartedly supporting my decision to pursue higher education in the U.S. and for their omnipresent hand of guidance and encouragement

And to Prof Jones, for his teaching and mentoring. If not for him I would not have attempted Finite Element for my thesis topic. I find immense inspiration in his ideals of “perseverance” and “guilt”.

Acknowledgements

I thank the Rose-Hulman Institute of Technology for giving me an opportunity to pursue my higher education in Mechanical Engineering. I am indebted to Rose for the help and support that I have obtained throughout my Master's education.

I sincerely thank my advisor Professor Jones for his omnipresent hand of guidance. His expertise in the world of Finite Element has always inspired me to dive into the deeper depths of Finite Element in Mechanical Engineering. Professor Jones's emphasis on conceptual and abstract thinking and his problem solving approach have expanded my thinking and changed my work habits. I deeply admire his work ethic and I seek to emulate it in my life.

I thank Professor Olson for inspiring me to extend my understanding of finite element into the real world and for giving me a chance to experiment with mechanical design.

I thank Professor Holder for his patient and prompt help. If not for him, I would not have been able to get along with understanding the indispensable skill of numerical computing and Matlab programming.

I thank Karen DeGrange for her helpful counsel throughout my Graduate study at Rose.

Finally, I thank Terri Gosnell, who has always been there for help and guidance on the Graduate Process at the Rose-Hulman Institute of Technology. I greatly appreciate her for her timely and supportive help.

Table of Contents

List of Figures

List of Abbreviations

FEM-Finite Element Methods

TFEM-Time Finite Element Methods

FDM-Finite Difference Methods

STFEM- Space Time Finite Element Methods

GM- Galerkin Method

CD – Central Differences

PDE-Partial Differential Equation

List of Tables

List of Symbols

χ – Displacement

ũ – Trial function

$\tilde{\upsilon}$ - weighting function

$\bar{X}$ - Ratio of element size to the total length of the bar

N - shape function

L - Length of bar

C - damping coefficient

q - Displacement corresponding to the time step

$\dot{q}$ - Velocity

$\ddot{q}$ - Acceleration

Δx - Difference between subsequent displacement values

Δt - Difference between subsequent time values

k - Stiffness

v_0 - Initial velocity

x_0 - Initial displacement

r, S, T - Auxiliary coordinates

ρ - Density

ω_n - Natural frequency

ω_d - Damping frequency

ζ - Analytic damping coefficient

C_1, C_2, C_3, C_4 - analytic constant

1. Introduction

Numerical techniques have been implemented to solve many engineering problems successfully in the past decades. Techniques exist with varying complexities for numerous problems, and the search for new, computationally efficient techniques has resulted in innovative formulations. This study investigates the applicability of the Space-Time finite element formulation to solve problems related to the field of elastodynamics. Chapter 2 reviews current literature on the subject. The workings of the Galerkin method are explained in Chapter 3, the concept of time discretization using finite elements for a single degree of freedom case is explored in Chapter 4, and finally Chapter 5 looks at space-time finite element discretization for an axially vibrating bar. The computed results are presented and compared with existing techniques, and we conclude in Chapter 6.

Implementing time discretization using finite elements has been of interest in the numerical computing society since 1987[3]. Accommodating time discretization along with space discretization in a single element formulation might result in greater accuracy and reduced computational time, especially in cases involving a specific time parameter, such as transient problems and dynamics. Many industries would benefit if computational efficiencies are improved, including the aero-engines industry. The following section introduces the academic framework and theoretical formulation of the Space-Time Finite Element Method (STFEM).

2. Literature Review

This chapter reviews the literature in the field of Space-Time Finite Element Methods (STFEM). To provide a fundamental understanding, the following sections present the development of the academic literature from the basic ideas to the present topic.

2.1 Introduction

The branch of physics that tries to understand the behaviour of continuous media due to forces and their respective displacements is called continuum mechanics [1]. This specific field has been developed as a result of the amalgamation of the two broad fields: solid mechanics and fluid mechanics [1]. Some areas with specific emphasis have been developed with respect to the nature of the applied force and the behaviour of solids with respect to these forces (*e.g.* statics, kinematics). Other areas have been developed with respect to the nature of displacement of the material (*e.g.* elastic and inelastic). The study of elastic solid behaviour under the influence of dynamic forces is the field of elastodynamics [2]. Broadly speaking, this field deals with the forces that cause the displacement of the medium to be in the form of waves. Problems like the impact of a rigid bar fixed to a wall, gradual force applied onto a spring and an impact force applied onto a spring where the displacements are in the elastic nature are dealt in the linear elastodynamics realm [2].

Many methods exist to solve elastodynamics problem, with Finite Element Methods (FEM) being one of the widely used numerical techniques. Innovative and sophisticated formulations have been developed and tested with the aim of improving accuracy and reducing computational time. The space-time finite element formulation is one such method [4].

2.2 Space Time

J.H.Argyris and D.W.Scharpf [3] in their seminal paper titled '*Finite Elements in Time and Space*', put forth the concept of finite element discretization for time dependent phenomena. They introduced the theoretical formulation of time discretization and elucidated the nature of time discretization. They state the idea of finite element in time discretization and explain how it translates to fixed time interval. They illustrate their concept through a unidirectional bar example and then extend it to multi-degrees of freedom.

Thomas J.R. Hughes and Gregory M. Hulbert [4], in their pivotal paper '*Space-Time Finite Element Methods for Elastodynamics: Formulations and Error Estimates*', systematise and formalise the time discretization idea into the space-time finite element method and apply it to classical elastodynamic problems. They present their analysis of the semi-discrete approach wherein space is first discretized using a finite element method and then time is discretized using a Finite Difference Method (FDM). They argue that it would be more efficient if time discretization is done using an FEM; STFEM could be used to circumvent the use of finite differences to develop systems of ordinary differential equations. They then explore a time discontinuous Galerkin formulation, which was developed for hyperbolic problems, and apply it to an elastodynamic example and present theoretical convergence analysis. Their formulation is used in various works either directly or in higher order approximations. In another paper titled '*Space-Time Finite Element Formulation for Second Order Hyperbolic Equations*' [5], they develop STFEM to be unconditionally stable and higher order accurate, in that orders of approximation higher than cubic degree can be used. They also point to advantages of the method like mathematically proving stability and convergence and extend the method to elastodynamics and higher order hyperbolic problems.

Donald A. French [6] takes the STFEM idea and applies it to the wave equation. In his work titled '*A space-time finite element method for the wave equation*' he introduces his

formulation and compares it with that of Thomas J.R. Hughes and Gregory M Hulbert. French claims that there is no need for extra least square terms in his formulation and that the convergence test holds for time slabs with arbitrary thickness. He also details a space-time method to solve the wave problem and estimates both predicted and computed errors. X.D. Li and N.E.Wiberg [7] published a study on the implementation and adaptivity of STFEM for 2D problems and they use bilinear basis functions that are discontinuous in time. They have effectively used adaptive meshes for the spatial and temporal dimension and have produced computationally efficient solutions.

Franck Jourdan, Serge Dumont, Tarik Madani published "*A Space-Time Finite Element Method for elastodynamics problems : elementary examples of 4D remeshing using simplex elements*" [8] in which they explore continuous Galerkin method in STFEM. They present continuous Galerkin method as an alternative to some problems that have been previously solved using discontinuous Galerkin. They compare the convergence characteristics and the stability of the method, and also include meshing. Mathew Anderson and Jung-Han Kimn [9] develop a numerical approach to STFEM for the wave equation using a continuous time Galerkin method and present a time decomposition strategy that results in improved performance of the program.

STFEM has been used successfully in fluid flow problems [10,11,12] and in impact problems [13]. STFEM has also been applied to elastodynamics problems [18]. For most studies the emphasis has been in using STFEM with discontinuous Galerkin methods, though they can be used with a continuous Galerkin approach equally well. The next chapter introduces the continuous Galerkin framework of this study.

3. Galerkin Method

3.1 Introduction

This chapter introduces the background of the Galerkin method, which is one of the numerical methods used for defining the finite element problem. The Galerkin method is one formulation of the weighted residual family [14]. The word residual is indicative of the numerical approximation involved in solving the problem.

There are two broad mathematical methods in which problems are solved, the analytical approach, which is also called the direct approach, and the variational approach [15]; the Galerkin method is a specialized method of the second type. The primary method used to solve a continuum mechanics problem is the direct approach [15]. The direct approach uses the governing equations constructed from the fundamental differential equations. The direct approach enables the derivation of a closed form solution, and hence, it is the benchmark to which methods are compared. When the results yielded by the direct approach and variational methods disagree, the difference is the residual. The weighted residual method employs mathematical tactics to minimize residuals obtained. The Galerkin approach is a specific weighted residual technique found to be more efficient in solving certain problems like those in elastodynamics [14].

3.2.1 Background on the Galerkin Approach

Many weighted residual techniques are used to solve differential equations, which some important techniques are point collocation, sub-domain collocation, and the Galerkin method [15]. The Galerkin method is preferred for the finite element formulation of problems in elastodynamics as this technique yields symmetric matrices, which increase numerical efficiency and decrease computational expenditure [14]. The Galerkin method uses two important functions called the trial function and the weighting function to approximate the

solution to the differential equation [15]. The trial function is the approximation applied to the direct approach and the weighting function acts to reduce the approximated error.

3.2.2 Finite Element Method

Solving for reactions in a solid component with complex geometry is difficult using just the direct approach [15]. In such cases, the geometry is discretized into individual-components, known as elements [15]. This is at the heart of the finite element method. The division of the global geometry into elements reduces the complexity of the problem [15]. Each finite element contains its own set of characteristic equations, which goes on to form the respective element matrix [15]. The characteristic matrices of the elements are coupled to generate the consolidated matrix of the global geometry, which can be written as follows:

$$[D]\{u\}=\{f\}, \tag{3.1}$$

where,

$[D]$ is the consolidated characteristic element matrix derived from the governing differential equation,

$\{u\}$ is the vector of the unknowns, and

$\{f\}$ is the characteristic force vector,

Once the problem is cast into the above form, many techniques can be used to solve the system of equations.

3.3 The Galerkin Finite Element Method in One Dimension

The direct approach of solving a problem uses the governing equation in its most fundamental differential equation [17]. The differential equation with the boundary conditions is known as the strong form [17]. The weak form has the differential equation

written as an integral and is an approximation of the strong form and its boundary conditions [17].

For example, in a linear stress analysis problem, the strong form of the static deformation equation for a one dimensional rod, which is fixed on one end and has a force acting on the other (as shown in figure (3.1)), is known from the following equation:

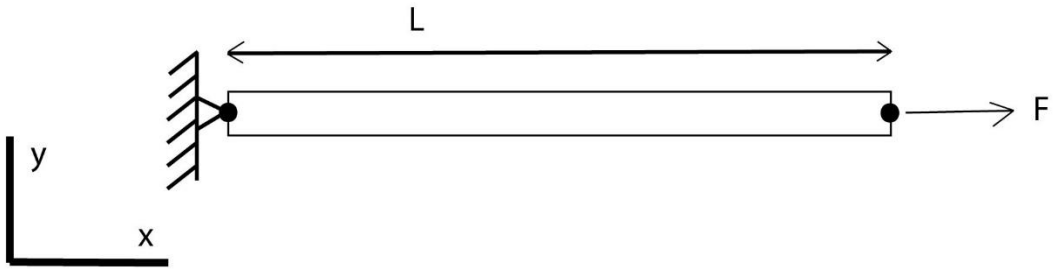

Fig 3.1 – 1-D rod pinned at one end and subjected to force on the other end.

$$\frac{d}{dx}\left(AE\frac{du}{dx} \right) = 0, \tag{3.2}$$

where *A* is the cross sectional area of the rod,

E is the elastic modulus,

u(x) is the displacement parameter, and

$\frac{du}{dx}$ is the axial strain,

The boundary conditions are $u(0) = 0$ and $\frac{du}{dx}(L) = \frac{F}{EA}$.

In the variational approach the weak form requires that the displacement parameter be approximated such that it satisfies the equation in an average sense; this approximation function is called the trial function $\tilde{u}(x)$ [14]. The solution obtained through the use of the trial function is an approximation, thus residual is obtained in general,

$$\frac{d}{dx}\left(AE\frac{d\tilde{u}}{dx} \right) = R\,. \tag{3.3}$$

The trial function can be multiplied with an arbitrary weight $\tilde{v}$ in order to reduce the residual, integrating over the whole domain to seek a result of zero [16]. The vector $\tilde{v}(x)$ is called the weighting function [16], and the goal is to reduce the residual to zero [16]. This technique is also called the weighted residual method [15]. Another property of the weighting function is that if, at a certain location, the value of $u(x)$ is known though the boundary condition, the weighting function's value is set to zero.

Multiplying equation (3.3) with the weighting function, and integrating over the domain,

$$\int_0^L \tilde{v}\left[\frac{d}{dx}\left(AE\frac{d\tilde{u}}{dx} \right) \right] dx = 0\,. \tag{3.4}$$

The transformed equation (3.4) is the Galerkin weak form. Expanding equation (3.4) and integrating by parts gives

$$\int_o^L \tilde{v}\frac{d}{dx}\left(EA\frac{d\tilde{u}}{dx} \right) dx = -\int_0^L \frac{d\tilde{v}}{dx}\left(EA\frac{d\tilde{u}}{dx} \right) dx + \tilde{v}\left(EA\frac{d\tilde{u}}{dx} \right)_L - \tilde{v}\left(EA\frac{d\tilde{u}}{dx} \right)_0 . \tag{3.5}$$

Enforcing the boundary conditions, we have

$$\int_o^L \tilde{v}\frac{d}{dx}\left(EA\frac{d\tilde{u}}{dx} \right) dx = -\int_0^L \frac{d\tilde{v}}{dx}\left(EA\frac{d\tilde{u}}{dx} \right) dx + \tilde{v}\left(EA\frac{d\tilde{u}}{dx} \right)_L . \tag{3.6}$$

In the expanded equation (3.6) we observe the application of the principle that if the boundary condition is known (*i.e.,* $\tilde{u}(0)$ is known), then the weighting function is reduced to zero (i.e., $\tilde{v}(0) = 0$), which results in a simplified equation. Another noticeable feature is that

the use of integration by parts allows the reduction of the order of the differential, ensuring the symmetry of the characteristic matrices of each element [16].

The Galerkin method is different from the other weighted residual methods because the weights $\tilde{v}_i$ are selected in terms of the trial solution such that the inner product of $\tilde{u}(x)$ and $\tilde{v}(x)$ is equal to zero [15]. The trial functions are approximated through admissible shape functions $N_i(x)$ such that $\tilde{u}(x) = \{N(x)\}^T \{a_n\}$, where $\{N(x)\}^T = \{N_1, N_2 ..... N_n\}$, and $\{a_n\} = \{a_1, a_2 ..... a_n\}$ is the notation for generalized degrees of freedom. Thus the weighting function is related to the trial function as the partial derivative of the trial function at every a_i, expressed as [15],

$$\tilde{v}_i = \frac{\partial \tilde{u}}{\partial a_i} = N_i(x). \qquad (3.7)$$

The following section deals with the shape functions and establishes the link between Galerkin method's trial and weighting functions and the geometry of the problem being analysed.

3.4 Shape Function

Shape functions express the solution within an element using polynomial approximation [15]. The trial and weighting functions are often constructed from shape functions. As such, it is critical to understand the fundamentals of the shape functions and their relation to the trial and weighting functions.

When a geometric domain is discretized, many finite elements are created. Shape functions are polynomials that approximate the solution of the weak form equation over the span of the elements [14]. The accuracy of the approximation increases with the order of the

polynomial [16]. A shape function of first-order results in a linear finite element [15]. Two types of shape functions are generally used (i) local and (ii) isoparametric [15]. Consider the shape function of the local linear element.

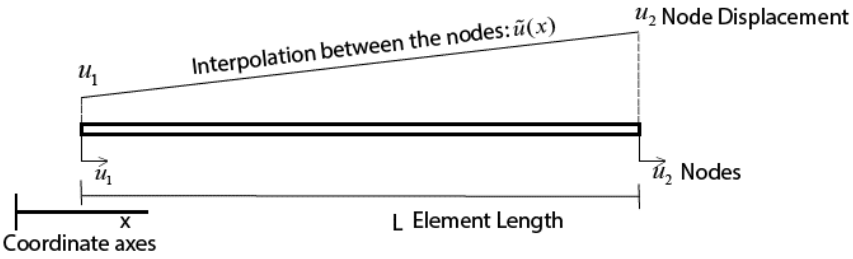

Fig 3.2: interpolation between nodal displacements in a linear element

Figure (3.2) illustrates a linear element with two nodes and the displacement undergone by the nodes due to an axial force acting along the element. It is assumed the displacement field over the element can be approximated as linear. The equation corresponding to Figure 3.2 is,

$$\tilde{u}(x) = \alpha_1 + \alpha_2\left(\frac{x}{L}\right), \tag{3.8}$$

where α_1 and α_2 are constants,

x is the variable length,

L is the length of the element, and

$\tilde{u}(x)$ is the assumed displacement field.

Defining $\bar{X} = \frac{x}{L}$ to be the local coordinate system, where $0 \le \bar{X} \le 1$, the equation (3.8) reduces to $\tilde{u}(x) = \alpha_1 + \alpha_2(\bar{X})$. (3.9)

At $\bar{X}$ = 0, $u(0) = u_1$ from Fig 3.2 and $u(0) = \alpha_1$ from equation (3.9) (3.10)

At $\bar{X}$ =1, $u(1) = u_1$ from Fig 3.2 and $u(1) = \alpha_1 + \alpha_2$ from equation (3.9) (3.11)

From equation (3.9) it can be noted that $\alpha_2 = u_2 - u_1$, (3.12)

Substituting the values obtained for α_1 and α_2 in equation (3.9) gives

$$\tilde{u}(x) = u_1 + (u_2 - u_1)(\bar{X}). \tag{3.13}$$

Grouping the nodal displacements from the above equation gives

$$\tilde{u}(\bar{X}) = u_1(1 - \bar{X}) + u_2(\bar{X}). \tag{3.14}$$

The above equation forms

$$\tilde{u}(\bar{X}) = \left\{(1 - \bar{X}), (\bar{X})\right\} \begin{Bmatrix} u_1 \\ u_2 \end{Bmatrix}. \tag{3.15}$$

Equation (3.15) can be written as

$$\tilde{u}(\bar{X}) = \left\{N(\bar{X})\right\}^T \{u_n\}. \tag{3.16}$$

where $\left\{N(\bar{X})\right\}$ is a vector of shape functions and $\{u_n\}$ is the nodal displacement vector.

Substituting $\tilde{u}$ for u in equation (3.3) results in

$$\frac{d}{dx}\left(EA \frac{d\left\{N(\bar{X})\right\}^T}{dx} \{u_n\} \right) = R. \tag{3.17}$$

The weighting function is,

$$\tilde{v}(\bar{X}) = \left\{N(\bar{X})\right\}. \tag{3.18}$$

Thus equation (3.4) is

$$\int_0^L \{N(\bar{X})\} \frac{d}{dx}\left(EA \frac{d\{N(\bar{X})\}^T}{dx} \{u_n\} \right) dx = 0 . \qquad (3.19)$$

Higher order shape functions can be computed in a similar fashion, the usual options being quadratic or cubic [17]. Shape functions are subjected to continuity and completeness assumptions before they are implemented for finite formulations [17]. Shape functions are also expected to uphold the convergence test as a fundamental requirement before the results obtained are considered authentic [17].

3.5 Discretization

Applying the linear element developed in Section 3.4 for a discretization, the bar is divided into 3 elements with equal length.

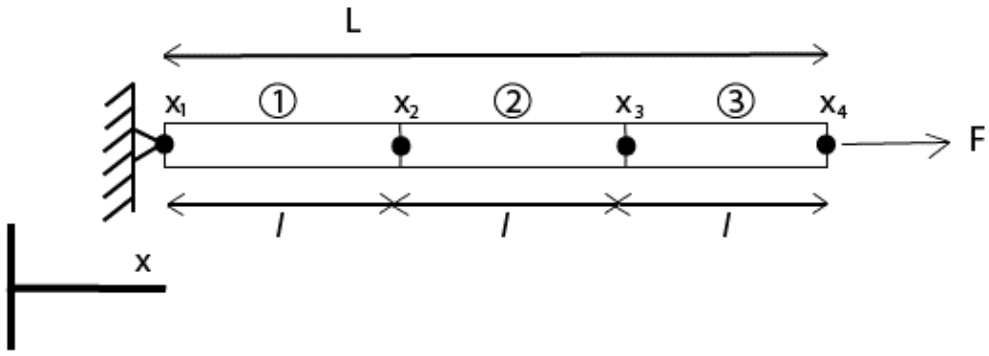

Fig 3.3 – Bar discretized into 3 elements and 4 nodes

The left end of the rod is pinned, in other words the displacement is zero. Therefore, after integration by parts, equation (3.19) reduces to,

$$\int_0^L \frac{d\tilde{v}}{dx}\left(EA \frac{d\tilde{u}}{dx} \right) dx = \tilde{v}(EA \frac{d\tilde{u}}{dx})|_L . \qquad (3.20)$$

Note that $d\tilde{u}/dx$ evaluated at L is equal to F/EA from Hooke's law under the elastic limit. Hence,

$$\int_0^L \frac{d\tilde{v}}{dx}\left(EA\frac{d\tilde{u}}{dx}\right)dx = \tilde{v}(L)F\ . \tag{3.21}$$

The integration limits for, equation (3.21) are separated according to the element discretization resulting in 3 separate terms that have their integral limits with respect to the element length. The resulting equation is

$$\int_{x_1}^{x_2} \frac{d\tilde{v}}{dx}(EA\frac{d\tilde{u}}{dx})dx + \int_{x_2}^{x_3} \frac{d\tilde{v}}{dx}(EA\frac{d\tilde{u}}{dx})dx + \int_{x_3}^{x_4} \frac{d\tilde{v}}{dx}(EA\frac{d\tilde{u}}{dx})dx = \tilde{v}(L)F\ . \tag{3.22}$$

Substituting the shape functions into the first term of the left hand side of equation (3.22) gives

$$\int_{x1}^{x2} \frac{d\left\{N(\bar{X})\right\}}{dx}\left(EA\frac{d\left\{N(\bar{X})\right\}^T}{dx}\begin{Bmatrix}u_1\\u_2\end{Bmatrix}\right)dx\ . \tag{3.23}$$

From equation (3.9) $\bar{X} = x/l$ and hence $d\bar{X}/dx = 1/l$, where $l = x_2 - x_1$ (3.24)

Applying the chain rule $d/dx = (d/d\bar{X})(d\bar{X}/dx)$ and equation (3.24) to equation (3.23):

$$EA\int_{x_1}^{x_2} \frac{1}{l}\frac{d}{d\bar{X}}\left\{N(\bar{X})\right\}\frac{1}{l}\frac{d}{d\bar{X}}\left\{N(\bar{X})\right\}^T dx\begin{Bmatrix}u_1\\u_2\end{Bmatrix}. \tag{3.25}$$

Performing a change of variable (χ to $\bar{X}$) and transforming the limits of integration from $[x_1, x_2]$ to [0,1] gives

$$\int_{x_1}^{x_2} dx = \int_0^1 l\,d\bar{X}\ . \tag{3.26}$$

Thus equation (3.25) becomes

$$\frac{EA}{l^2}\frac{d}{d\bar{X}}\begin{Bmatrix}1-\bar{X}\\ \bar{X}\end{Bmatrix}\frac{d}{d\bar{X}}\begin{Bmatrix}1-\bar{X}\\ \bar{X}\end{Bmatrix}^T\int_0^1 l d\bar{X}\begin{Bmatrix}u_1\\ u_2\end{Bmatrix}. \tag{3.27}$$

The result is the characteristic element stiffness matrix multiplied by the displacement vector

$$\frac{EA}{l}\begin{pmatrix}1 & -1\\ -1 & 1\end{pmatrix}\begin{Bmatrix}u_1\\ u_2\end{Bmatrix}. \tag{3.28}$$

Rewriting the equation (3.22) as

$$\frac{EA}{l}\begin{pmatrix}1 & -1\\ -1 & 1\end{pmatrix}\begin{Bmatrix}u_1\\ u_2\end{Bmatrix}+\frac{EA}{l}\begin{pmatrix}1 & -1\\ -1 & 1\end{pmatrix}\begin{Bmatrix}u_2\\ u_3\end{Bmatrix}+\frac{EA}{l}\begin{pmatrix}1 & -1\\ -1 & 1\end{pmatrix}\begin{Bmatrix}u_3\\ u_4\end{Bmatrix}=\tilde{v}(L)F\,. \tag{3.29}$$

Substituting the functions into the right-hand side of equation (3.21), the element force vector is obtained for the final element.

$$\tilde{v}(L)F=\left.\begin{Bmatrix}1-\bar{X}\\ \bar{X}\end{Bmatrix}\right|_{\bar{X}=1}F$$

$$\Rightarrow \qquad \tilde{v}(L)F=\begin{Bmatrix}0\\ F\end{Bmatrix}. \tag{3.30}$$

The direct assembly method [17] is applied to equations (3.29) and (3.31) resulting in

$$\frac{EA}{l}\begin{bmatrix}1 & -1 & 0 & 0\\ -1 & 2 & -1 & 0\\ 0 & -1 & 2 & -1\\ 0 & 0 & -1 & 1\end{bmatrix}\begin{Bmatrix}u_1\\ u_2\\ u_3\\ u_4\end{Bmatrix}=\begin{Bmatrix}0\\ 0\\ 0\\ F\end{Bmatrix}, \tag{3.31}$$

Equation (3.31) can be expressed in the fundamental form of equation (3.1), where the left-hand side of (3.31) contains the characteristic global matrix [D], the {u} vector, and the right-hand side contains the force vector {f}.

3.6 Isoparametric Shape Functions

Another type of shape function that is often used for meshing the physical domain is the isoparametric shape [15]. The global mesh is mapped onto an auxiliary domain; for a 1D case, the isoparametric elements domain spans $-1 \le r \le 1$ [15]. The isoparametric element is preferred over the global coordinated element as numerical integration is easier over a standard boundary than over a globally meshed boundary. Following section details the working of the 1D and 2D elements in greater detail.

3.6.1 The 1D Element

Isoparametric functions spans the auxiliary space $-1 \le r \le 1$. For a linear 1D element there are 2 nodes and 2 associated axial degrees of freedom element (u_1, u_2); the displacement field is approximated as $\tilde{u}(r) = N_1 u_1 + N_2 u_2$.

The isoparametric shape functions are

$$N_1 = \frac{1}{2}(1-r) \quad \text{and}$$

$$N_2 = \frac{1}{2}(1+r) \tag{3.33}$$

Which are shown graphically in Figure 3.4

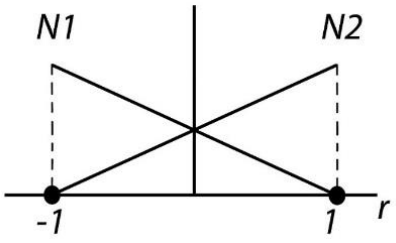

Fig 3.4 - Isoparametric linear element

For a quadratic isoparametric element, there are three nodes and three axial degrees of freedom (u_1, u_2, u_3). The first and the last nodes have coordinates -1 and 1, respectively, and

the middle node typically assumes the centre of the auxiliary domain (*i.e.*, node 2 at $r = 0$) for the quadratic element [16]. The quadratic shape functions are as follows

$$N_1 = \frac{-r}{2}(1-r),\ N_2 = 1-r^2 \text{ and } N_3 = \frac{r}{2}(1+r). \qquad (3.35)$$

The following would be the quadratic shape functions visualised.

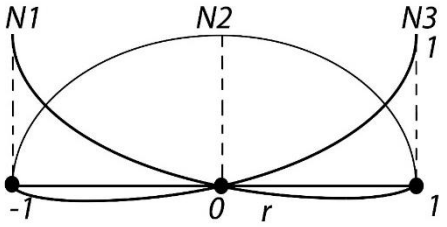

Fig 3.5 The isoparametric quadratic element

3.6.2 2D element

For 2D elements, a Jacobian matrix is used [15] to map between global and auxillary coordinate systems. The Jacobian matrix for a linear quadrilateral element is a two-by-two matrix of partial derivatives with respect to the auxiliary coordinates. The Jacobian scales the area of the auxiliary element to equal the physical element [15]. For linear quadrilateral elements the determinant of the Jacobian is always equal to $A/4$, where A is the area of the global element.

For 2D discretization, the element used is a quadrilateral bilinear isoparametric element. Space-Time discretization requires the element to be divided into time and space axes respectively, hence the horizontal axis is considered as space and the vertical as time. The following is the diagrammatic representation of the bilinear quadrilateral isoparametric element.

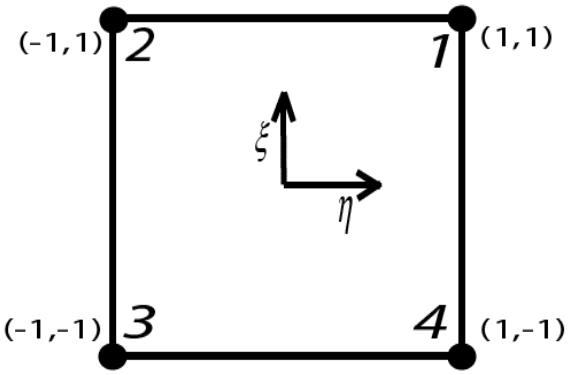

Fig 3.6 – Bilinear quadrilateral isoparametric element with nodes numbered

The shape functions for the quadrilateral element [15] are,

$$\{N(\eta,\xi)\} = \begin{Bmatrix} \frac{1}{4}(1+\eta)(1+\xi) \\ \frac{1}{4}(1-\eta)(1+\xi) \\ \frac{1}{4}(1-\eta)(1-\xi) \\ \frac{1}{4}(1+\eta)(1-\xi) \end{Bmatrix}, \tag{3.36}$$

Further details on the isoparametric element and the development of constituent matrices are available in Robert Cook *et al. "Concepts and Applications of Finite Element Analysis"*[15] and in "*Finite Element Method in Engineering*" by S.S.Rao [17].

4. Time Formulation in Single Degree of Freedom

As a preliminary step, a simple case involving pure time discretization is considered. In this section the model is described, and the analytical response is presented. Then a central difference method is used to approximate the solution. A Time Finite Element Method (TFEM) formulation is also employed using both linear and quadratic elements. The obtained results are compared to analytic and central difference results.

4.1 The Model

The single degree of freedom model considered is a mass-spring-damper system. The mass is constrained to move purely in the *x* direction as shown in figure 4.1

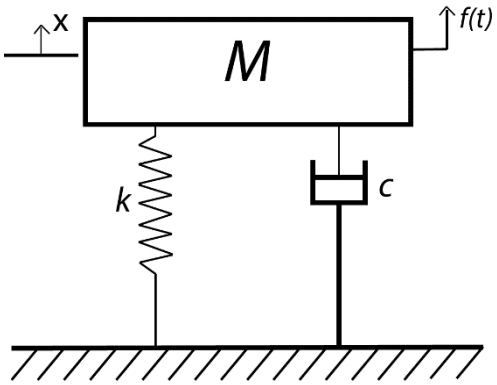

Fig 4.1 – Mass on Spring Single Degree of Freedom Model

Here m is the mass, k is the stiffness, c is the damping coefficient, x is the displacement of the mass, and $f(t)$ is the harmonic force acting on the block. The governing equation of motion is

$$m\ddot{x} + c\dot{x} + kx = f_0 \sin(\omega t). \tag{4.1}$$

The block exhibits simple harmonic motion, where $\ddot{x}$ is the acceleration of the block, $\dot{x}$ is the velocity, ω is the forcing frequency, and t is the time variable. The solution to equation (4.1) is [20]:

$$x_T(t) = e^{-\zeta\omega_n t}\left(C_1 \cos(\omega_d t) + C_2 \sin(\omega_d t)\right) + C_3 \cos(\omega t) + C_4 \sin(\omega t), \tag{4.2}$$

where C_1, C_2, C_3, C_4 are constants determined from the initial and loading conditions, ς is the damping ratio, ω_d is the damped natural frequency and ω is the forcing frequency. Further details are provided in Appendix A.

4.2 Time Stepping

The finite difference scheme is a common numerical method used to approximate the solutions to such transient problems [14]. The solution to the ordinary differential equation is approximated through a finite difference calculation where the required derivatives are approximated using the difference between displacement values at discrete values of x. There are many such methods with Central Differences (CD) being one possibility [14]. The forward time stepping scheme for a Single Degree of Freedom (SDOF) model is

$$q_{i+1} = \left(\frac{m}{\Delta t^2} + \frac{c}{2\Delta t} \right)^{-1} \left[f_i - q_i \left(\frac{m}{\Delta t^2} + k \right) - q_{i-1} \left(\frac{m}{\Delta t^2} - \frac{c}{2\Delta t} \right) \right], \tag{4.3}$$

where m is the mass,

c is the damping coefficient,

Δt is the time step,

f_i is the forcing amplitude at time step *i*,

q_i is the value of displacement at the corresponding time step,

q_{i-1} is the value of displacement at the previous time step, and

q_{i+1} is the value of displacement at the subsequent time step.

The displacement at both the previous and current time steps are necessary in order to find the displacement in the next time step. The CD method is sensitive to the value of the time

step Δt, and it is found that the CD method is stable for Δt values less than $\left(2/\omega_{\max}\right)$, where $\omega_{\max}$ is the maximum natural frequency of the system [16]. For continued development of CD technique, please refer to Appendix B and *Introduction to Numerical Analysis* by James Efferson [19].

4.3 Time Finite Element Method

In this section the Time Finite Element Method (TFEM) is expressed with linear and quadratic elements. Results are discussed in the following section. Solving the damped mass-on-spring problem with the FET requires approximating (4.1) with a trial function,

$$m\ddot{\tilde{u}} + c\dot{\tilde{u}} + k\tilde{u} = f_0 \sin(\omega t). \tag{4.4}$$

The weighting function is then applied and the inner product taken

$$\int_0^T \tilde{v}\left(m\ddot{\tilde{u}} + c\dot{\tilde{u}} + k\tilde{u} - f_0 \sin(\omega t)\right)dt = 0\ . \tag{4.5}$$

Expanding this equation and integrating by parts,

$$-\int_0^T \dot{\tilde{v}} m\dot{\tilde{u}}dt + \left[\tilde{v}m\dot{\tilde{u}}\right]_0^T + \int_0^T \tilde{v}\left(c\dot{\tilde{u}}\right)dt + \int_0^T \tilde{v}\left(k\tilde{u}\right)dt = \int_0^T \tilde{v}\left(f_0 \sin\left(\omega t\right)\right)dt\ . \tag{4.6}$$

From the above equation the terms for element mass [*M*], stiffness [*K*], damping [*C*] matrices and forcing {*F*} vector and the boundary condition terms are known,

$$[M] \text{ from } = \int_0^T \dot{\tilde{v}} m\dot{\tilde{u}}dt\ , \tag{4.7}$$

$$[K] \text{ from } = \int_0^T \tilde{v}\left(k\tilde{u}\right)dt\ , \tag{4.8}$$

$$[C] \text{ from } = \int_0^T \tilde{v}\left(c\dot{\tilde{u}}\right) dt, \tag{4.9}$$

$$\{F\} \text{ from } = \int_0^T \tilde{v}\left(f_0 \sin\left(\omega t\right)\right) dt \text{, and} \tag{4.10}$$

$$\text{The boundary condition terms } = \left[\tilde{v}m\dot{\tilde{u}}\right]_0^T \Rightarrow BC_1 = \left[\tilde{v}m\dot{\tilde{u}}\right]_T \ \& \ BC_2 = \left[\tilde{v}m\dot{\tilde{u}}\right]_0 \tag{4.11}$$

Note that these terms remain the same for both linear and quadratic elements.

4.3.1 Linear elements

The linear shape functions are used first to define the trial and weighting functions. Consider the following shape functions,

$$\left\{N\left(r\right)\right\} = \begin{Bmatrix} \dfrac{1-r}{2} \\ \dfrac{1+r}{2} \end{Bmatrix}. \tag{4.12}$$

where r in (4.12) maps to time in TFEM formulation. Defining $\tilde{u}\left(r\right) = \left\{N(r)\right\}^T \{u_n\}$ and $\tilde{v}(r) = \left\{N(r)\right\}$ and substituting the shape functions in (4.7) to (4.11) and performing the integrations, the following matrices are obtained.

$$[M] = \frac{m}{\Delta t}\begin{bmatrix} 1 & -1 \\ -1 & 1 \end{bmatrix}, \tag{4.13}$$

$$[K] = \frac{k\Delta t}{6}\begin{bmatrix} 2 & 1 \\ 1 & 2 \end{bmatrix}, \text{ and} \tag{4.14}$$

$$[C] = \frac{c}{2}\begin{bmatrix} -1 & 1 \\ -1 & 1 \end{bmatrix}. \tag{4.15}$$

A full derivation is provided in Appendix C. The above terms for the element matrices are coupled to global assembled matrix.

$$([K]_G + [C]_G - [M]_G)u + [\tilde{v}m\dot{\tilde{u}}]_T = F + [\tilde{v}m\dot{\tilde{u}}]_0, \qquad (4.16)$$

$$\begin{pmatrix} a & b & 0 & \cdots & 0 \\ c & d+a & b & 0 & \vdots \\ 0 & \ddots & \ddots & \ddots & \vdots \\ \vdots & 0 & \ddots & \ddots & b \\ 0 & 0 & \cdots & c+\frac{mk_1}{\Delta t} & d+\frac{mk_2}{\Delta t} \end{pmatrix} \begin{pmatrix} u_1 \\ u_2 \\ \vdots \\ \vdots \\ u_n \end{pmatrix} = \begin{pmatrix} f_1 + mv_0 \\ f_2 \\ \vdots \\ \vdots \\ f_n \end{pmatrix}. \qquad (4.17)$$

The boundary condition term $[\tilde{v}m\dot{\tilde{u}}]_T$ from equation (4.11) is associated with the last element and reduces into a matrix $\frac{m}{\Delta t}\begin{pmatrix} 0 & 0 \\ k_1 & k_2 \end{pmatrix}\begin{Bmatrix} u_{n-1} \\ u_n \end{Bmatrix}$ which is added to the assembled matrix. The other boundary condition term $[\tilde{v}m\dot{\tilde{u}}]_0$ is associated with the first element and reduces to $\begin{Bmatrix} mv_0 \\ 0 \end{Bmatrix}$, where v_0 is the initial velocity; it is added to the forcing vector as shown in equation (4.17). For detailed derivation of the boundary condition matrices please refer to Appendix C.

It can be noted that initial displacement has to be enforced in the system of equations. This is done by introducing a new row into the system of equations for the equation $u_1 = x_0$. Following changes are introduced to equation (4.17) .

$$\begin{pmatrix} a & b & 0 & \cdots & 0 \\ c & d+a & b & 0 & \vdots \\ 0 & \ddots & \ddots & \ddots & \vdots \\ \vdots & \ddots & \ddots & \ddots & b \\ 0 & \cdots & \cdots & c+k_1 & d+k_2 \\ 1 & \cdots & \cdots & \cdots & 0 \end{pmatrix} \begin{pmatrix} u_1 \\ u_2 \\ \vdots \\ \vdots \\ u_n \\ \end{pmatrix} = \begin{pmatrix} f_1 + mv_0 \\ f_2 \\ \vdots \\ \vdots \\ f_n \\ x_0 \end{pmatrix}. \qquad (4.18)$$

Introducing the extra constraint equation has the effect of making the system of equations rectangular of size [*n+1*,*n*]. Hence a row is arbitrarily chosen and eliminated to

regain the square [*n*,*n*] configuration. The nth row is chosen for elimination and resulting in the following system of equations.

$$\begin{pmatrix} a & b & \cdots & \cdots & 0 \\ c & d+a & b & \cdots & 0 \\ 0 & \ddots & \ddots & \ddots & \vdots \\ \vdots & 0 & \ddots & \ddots & b \\ 1 & 0 & \cdots & 0 & 0 \end{pmatrix} \begin{pmatrix} u_1 \\ u_2 \\ \vdots \\ \vdots \\ u_n \end{pmatrix} = \begin{pmatrix} f_1 + mv_0 \\ f_2 \\ \vdots \\ \vdots \\ x_0 \end{pmatrix} \tag{4.19}$$

Among the methods available in solving the linear system of equations, the block matrix inverse method is popular but computationally expensive. Other widely used methods include the LU decomposition, Cholesky decomposition, and algorithmic solving. The algorithmic solving would involve iteratively stepping through the assembled matrix while solving for the unknown. When compared with the block matrix inverse, algorithmic solving has the significant advantage of being computationally efficient, but formulating a solvable iterative algorithm is complex. An example of such iterative algorithm is provided in [18].

4.3.2 Quadratic elements

In order to better understand the impact of higher order approximations on attributes like computational performance and accuracy, the element complexity is increased to a quadratic formulation. The following would be the shape functions for a quadratic formulation [16],

$$\left\{N\left(r\right)\right\} = \begin{Bmatrix} \dfrac{-r(1-r)}{2} \\ 1-r^2 \\ \dfrac{r(1+r)}{2} \end{Bmatrix}, \tag{4.20}$$

as is described in Section 3.6. Using the above formulation the following element matrices are obtained, from equations (4.7)-(4.9)

$$[M] = \frac{m}{6\Delta t}\begin{pmatrix} 7 & -8 & 1 \\ -8 & 16 & -8 \\ 1 & -8 & 7 \end{pmatrix}, \tag{4.21}$$

$$[K] = \frac{k\Delta t}{15}\begin{bmatrix} 4 & 2 & -1 \\ 2 & 16 & 2 \\ -1 & 2 & 4 \end{bmatrix}, \text{ and} \tag{4.22}$$

$$[C] = \frac{c}{6}\begin{bmatrix} -3 & 4 & -1 \\ -4 & 0 & 4 \\ 1 & -4 & 3 \end{bmatrix}, \tag{4.23}$$

where Δt is the increment between nodes (i.e., the quadratic element has a total length of $2\Delta t$) the assembled matrix is.

$$\begin{pmatrix} a & b & c & 0 & \cdots & \cdots & 0 \\ d & e & f & 0 & \cdots & \cdots & \vdots \\ g & h & i+a & b & c & & \vdots \\ 0 & 0 & d & \ddots & \ddots & & \\ \vdots & \vdots & g & \ddots & i+a & b & c \\ \vdots & \vdots & & & d & e & f \\ 0 & \cdots & & & g+k_1 & h+k_2 & i+k_3 \end{pmatrix} \begin{Bmatrix} u_1 \\ u_2 \\ u_3 \\ \vdots \\ \vdots \\ \vdots \\ u_n \end{Bmatrix} = \begin{Bmatrix} f_1 + mv_0 \\ f_2 \\ f_3 \\ \vdots \\ \vdots \\ \vdots \\ f_n \end{Bmatrix} \tag{4.24}$$

Equation (4.23) is transformed in the same manner as applied to (4.18) to include the initial conditions. See Appendix D for details.

$$\begin{pmatrix} a & b & c & 0 & \cdots & \cdots & 0 \\ d & e & f & 0 & \cdots & \cdots & \vdots \\ g & h & i+a & b & c & & \vdots \\ 0 & 0 & d & \ddots & \ddots & & \\ \vdots & \vdots & g & \ddots & i+a & b & c \\ \vdots & \vdots & & & d & e & f \\ 1 & \cdots & & & 0 & 0 & 0 \end{pmatrix} \begin{Bmatrix} u_1 \\ u_2 \\ u_3 \\ \vdots \\ \vdots \\ \vdots \\ u_n \end{Bmatrix} = \begin{Bmatrix} f_1 + mv_0 \\ f_2 \\ f_3 \\ \vdots \\ \vdots \\ \vdots \\ x_0 \end{Bmatrix} \tag{4.25}$$

4.4 Results

This section presents the model properties, vibration response graphs, and the comparisons among the numerical techniques. Table 4.1 details the model properties used.

Tab 4.1 – Model properties used for the mass-spring-damper problem

Category	**Value**
Mass m	1 kg
Damping c	1 kg/s
Stiffness k	1000 N/m
Initial velocity v_0	1 m/s
Initial displacement x_0	1 m
Forcing frequency ω	2π rad/s
Initial force f_0	10 N

The response graph for the mass on spring model is given in Fig 4.2.

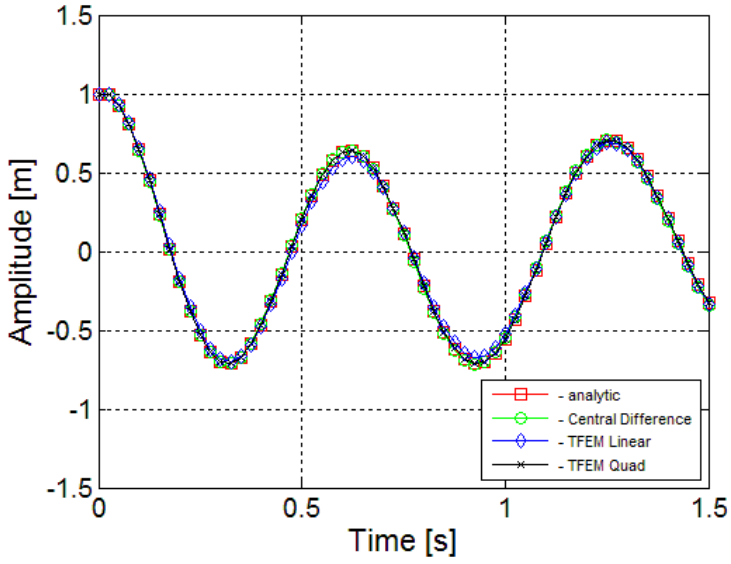

Fig 4.2 – The response graph for the mass-spring-damper single degree of freedom model ($\Delta t = 0.01s$)

In figure 4.2 it can be seen that the results from the central difference, TFEM linear and TFEM quadratic methods converge to the analytical solution. In order to better understand the convergence characteristics of the different methods, the total time taken for each time step (Δt) and the relative error between the methods are noted and compared.

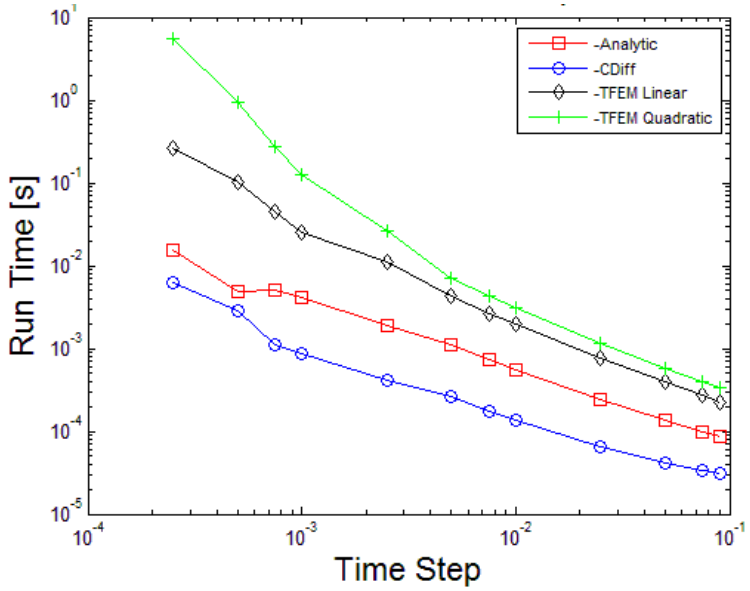

Fig 4.3 – Comparison between run time taken for each method vs time step (Δt)

It can be seen from figure 4.3 that as the time step decreases, all four methods exhibit an increase in total time. Central difference, analytical and TFEM linear exhibit slight increase in total time; TFEM quadratic exhibits a steeper increase in total time as time steps decrease. The values for the run time are found by taking average run time for 5 runs. It can be noticed that TFEM quadratic takes an order of magnitude more than the TFEM linear method and 2 orders of magnitude more than Central Difference; in other words requires greater computational expenditure when compared to TFEM linear and Central Difference. It is of interest to notice that the analytical method is slower than the Central Difference. This can be attributed to the fact that analytical method requires calculating the particular and harmonic solutions for every time step, whereas the Central Difference calculates only displacement for every time step. It is also of interest to note that Central Difference method

performs better than TFEM linear: as time steps decrease the total time taken for Central Difference is lesser than TFEM linear.

Relative error is calculated by taking the median of the difference between the analytical and the numerical methods. The next graph compares relative error between the three methods versus time step.

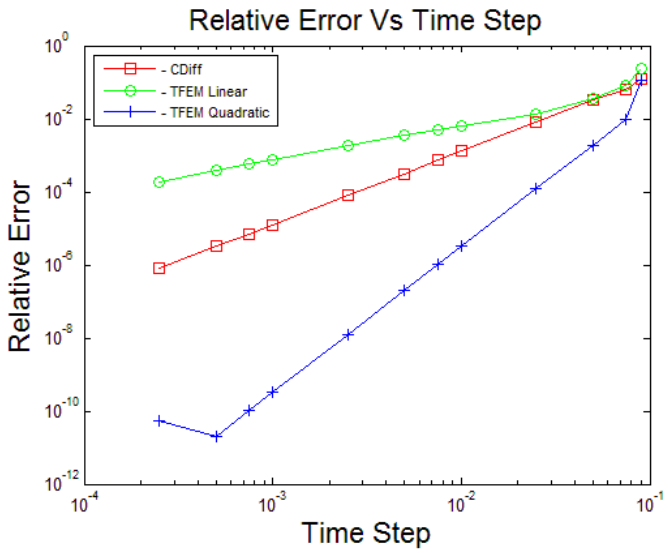

Fig 4.4 – Comparison between relative error and time step

From Fig 4.4, it can be seen that all the methods exhibit a linear downward trend. Central Difference yields relative error to the magnitude of 10^{-5} and is an order of magnitude more accurate for the same time steps when compared to TFEM linear, whereas TFEM quadratic is the most accurate when compared with Central Difference and TFEM linear with the relative error obtained by TFEM quadratic is 10^{-11}. From figure 4.3, it was noted that TFEM quadratic has the highest computational time requirement but from figure 4.4 it can also be noted that it is the most accurate method.

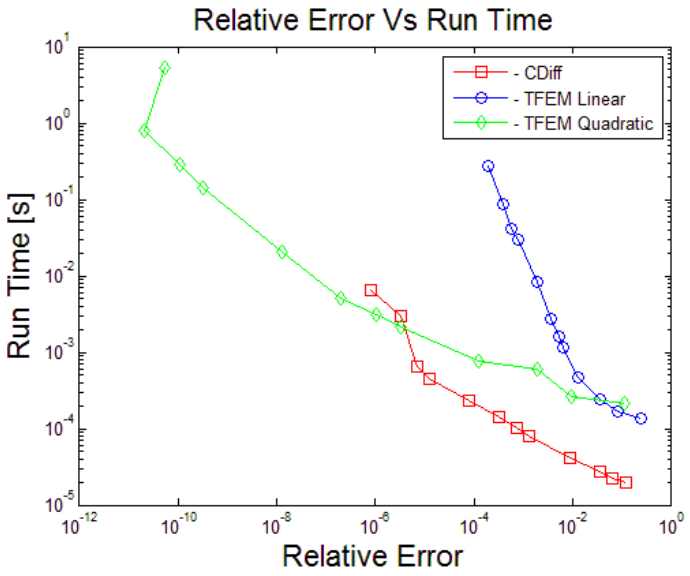

Fig 4.5 – Comparison between elapsed time vs relative error

From Fig 4.5, it can be seen that all three methods exhibits an increase in total time as relative error decreases. The TFEM linear curve exhibits an increase in total time with respect to decrease in error but when compared to Central Difference, TFEM linear takes longer time and also has higher error. The TFEM quadratic curve exhibits a steady increase in total time as the error decreases. TFEM quadratic yields the lowest error of the three methods but has higher computational time requirements. It is also of interest to identify the efficient frontier, which can be defined as the curve that is most efficient in terms of time and accuracy among the methods compared [21]. The quadratic method dominates the efficient frontier as it yields more accurate results of the three methods and while the central difference method is the fastest method, it is not remarkably fast.

4.5 Conclusion

From the above results it can be observed that Central Difference has relatively better accuracy for lesser time requirement when compared to TFEM linear. If the comparison is made purely from computational time perspective then Central Difference method fairs better than Time Finite Element method. If a method has to be chosen among the three presented methods based on optimality of performance then TFEM quadratic could be recommended as it is the efficient frontier.

It should be noted that these conclusions are dependent on the type of solver being used. The relative error of the methods is inherent to the numerical method and time step, whereas the run time of the TFEM is likely adversely affected by the direct solution approach. Iteratively solving the TFEM system of equations is predicted to significantly reduce computational time. This concept is discussed further in Chapter 6.

5. Space Time Formulation for an axially vibrating bar

5.1 Introduction

This chapter deals with the implementation of the Space Time Finite Element Method (STFEM) in an axially vibrating bar. Central Difference is used to approximate the response of the bar and tested for convergence over a range of mesh densities. The converged mesh is then used as a benchmark against which different mesh densities of SFTEM are tested. The converged results and the computational time of STFEM are presented and compared in the results section and conclusions are drawn from the obtained results.

5.2 Axially Vibrating Bar

While with a single degree of freedom the discretization is wholly in time, in the present case the bar must be meshed in both space and time. Consider the thin uniform bar depicted in Fig 5.1. In standard FEM, this bar is meshed using 1D bar elements in the spatial dimension. In STFEM, a 2D surface is used to represent the bar, where the horizontal direction accounts for the spatial dimension, and the vertical direction accounts for the temporal dimension.

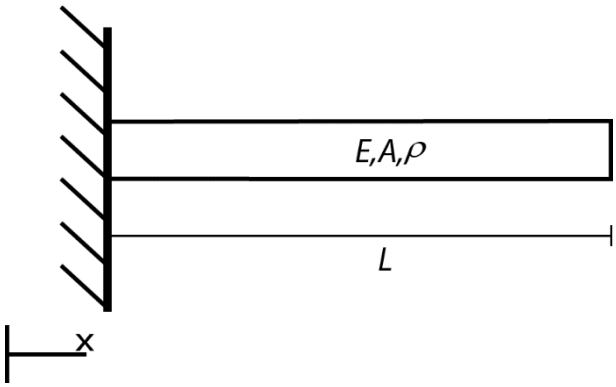

Fig 5.1 – axially vibrating Bar

The bar is rigidly fixed to a wall on the left and is stress free on the right. The bar is excited using an initial displacement and velocity.

The uniqueness of the Space-Time technique is the application of finite element discretization in the time dimension along with the space dimension. Discretizational similarity between central differences (a Finite Difference technique) and the Space-Time method lends itself to comparing and contrasting between both for better accuracy and computational efficiency. Discretization is done using bilinear quadrilateral elements for shape functions as described in Chapter 3.

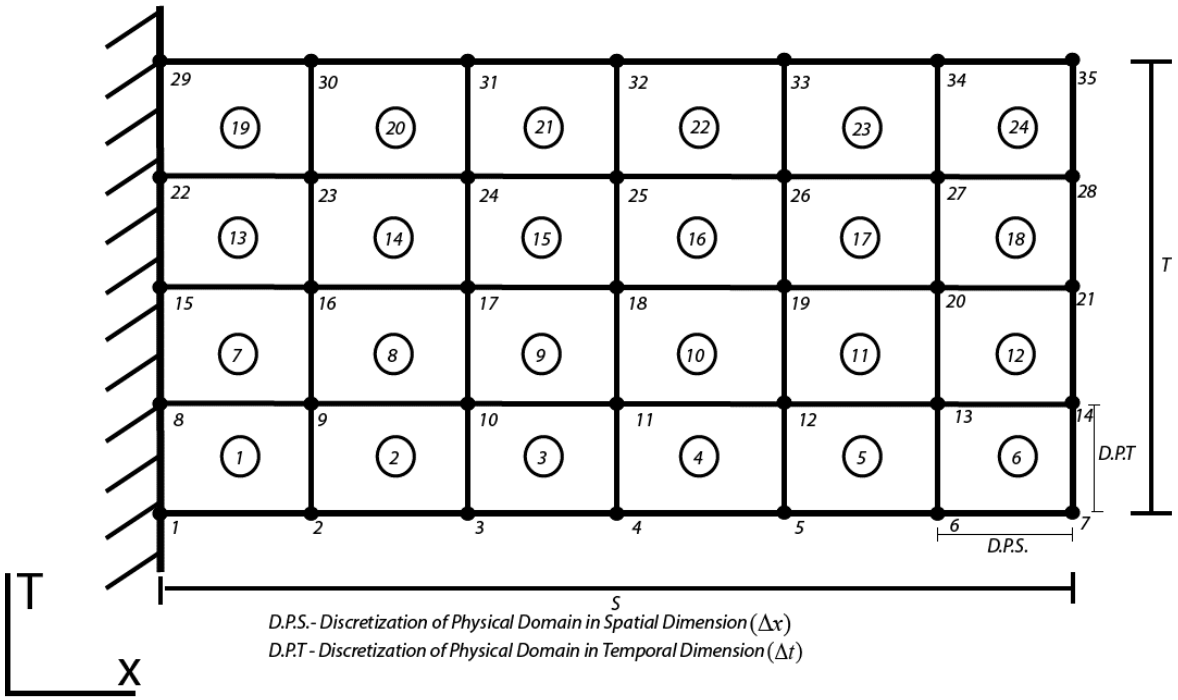

Fig 5.2 –Discretized bar in space and time where circled numbers represent elements and plain numbers represent nodes

In the above figure, the bar is discretized into 35 nodes and 24 bilinear quadrilateral elements. Space-Time discretization requires that each element has a spatial dimension and a temporal dimension. Due to this requirement, the length of the discretised model is considered to be in spatial dimension and the height of the model is in temporal dimension. Each node has a single degree of freedom: axial deflection $u(x,t)$.

The governing equation for a uniform, axial bar is given by the following equation

$$EA\frac{\partial^2 u}{\partial x^2} - \rho A\frac{\partial^2 u}{\partial t^2} + f = 0. \tag{5.1}$$

To apply the Space-Time method, the above equation is converted into a weak form with multiple integrals. The f term in equation (5.1) is ignored as no body loads are considered. The weak form of equation (5.1) is

$$\int_0^T \int_0^L \tilde{v}\left(EA\frac{\partial^2 \tilde{u}}{\partial x^2} - \rho A\frac{\partial^2 \tilde{u}}{\partial t^2} \right) dxdt = 0. \tag{5.2}$$

Expanding (5.2) using two integrations by parts gives

$$-\int_0^T \int_0^L EA\frac{\partial \tilde{v}}{\partial x}\frac{\partial \tilde{u}}{\partial x} dsdt + \left[\int_0^T EA\tilde{v}\frac{\partial \tilde{u}}{\partial x} \right]_0^L - \left(-\int_0^T \int_0^L \rho A\frac{\partial \tilde{v}}{\partial t}\frac{\partial \tilde{u}}{\partial t} dsdt + \left[\int_0^L \tilde{v}\rho A\frac{\partial \tilde{u}}{\partial t} dsdt \right]_0^T \right) = 0. \tag{5.3}$$

The element stiffness $[K]$ and mass matrices $[M]$ are derived along with the forcing vector {f} and initial conditions are isolated from equation (5.3):

$$[K] = \int_0^T \int_0^L EA\frac{\partial \tilde{v}}{\partial x}\frac{\partial \tilde{u}}{\partial x} dxdt. \tag{5.4}$$

$$[M] = \int_0^T \int_0^L \rho A\frac{\partial \tilde{v}}{\partial t}\frac{\partial \tilde{u}}{\partial t} dxdt. \tag{5.5}$$

Temporal Boundary Conditions (TBC) = $\left[\int_0^L \rho A\tilde{v}\frac{\partial \tilde{u}}{\partial t} dx \right]_{t=0}$, $\left[\int_0^L \rho A\tilde{v}\frac{\partial \tilde{u}}{\partial t} dx \right]_{t=T}$,

Spatial Boundary Conditions (SBC) = $\left[\int_0^T EA\tilde{v}\frac{\partial \tilde{u}}{\partial x} dt \right]_{x=0}$, $\left[\int_0^T EA\tilde{v}\frac{\partial \tilde{u}}{\partial x} dt \right]_{x=L}$. (5.6)

From the above boundary conditions, the term $\left[\int_0^T EA\tilde{v}\frac{\partial\tilde{u}}{\partial x}dt\right]_{x=0}$ reduces to zero as the value of displacement at x=0 is known thus the weighting function is set to zero. The term $\left[\int_0^T EA\tilde{v}\frac{\partial\tilde{u}}{\partial x}dt\right]_{x=L}$ would form the forcing vector but as no forcing is applied in the present model, the forcing vector is reduced to zero. The term $\left[\int_0^L \rho A\tilde{v}\frac{\partial\tilde{u}}{\partial t}dx\right]_{t=0}$ accounts for the initial velocity which is applied to the bottom set of nodes in Fig 5.3. For step by step details on derivation of this term please refer Appendix E. The term $\left[\int_0^L \rho A\tilde{v}\frac{\partial\tilde{u}}{\partial t}dx\right]_{t=T}$ results in terms to be applied at $t=T$ (*i.e.*, the top surface on Fig 5.3); in the process of constraining the system of equations, the rows associated with $t=T$ are chosen for elimination, so these terms are negated. Figure 5.3 graphically illustrates where all the boundary conditions are applied.

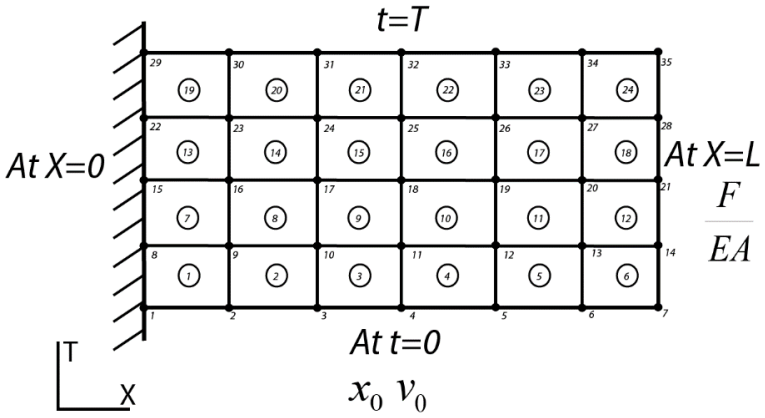

Fig 5.3 – Initial and Boundary conditions applied on the bar

From Figure 5.3 it can be noted that the initial conditions are applied at the bottom layer of nodes where $t=0$. In this depiction, both initial velocity and initial displacement are applied along nodes 1 through 7. The initial displacement is applied though the formula $x_0 \sin\left(\frac{\pi x_i}{2l}\right)$, where x_i is the respective spatial position, x_0 is the displacement amplitude and l

is the length of the bar the initial velocity is assumed to be constant across all nodes 1 through 7. For details on application of initial conditions please refer to Appexdix E.

To determine the element mass and stiffness matrices, the terms in equations (5.4)-(5.6) are approximated using the bilinear shape functions introduced in equation (3.36). Matrix derivation details are provided in Appendix E. The following element matrices are obtained:

$$[K] = \frac{EA}{6}\frac{\Delta t}{\Delta x}\begin{pmatrix} 2 & -2 & -1 & 1 \\ -2 & 2 & 1 & -1 \\ -1 & 1 & 2 & -2 \\ 1 & -1 & -2 & 2 \end{pmatrix} \quad \text{and} \quad (5.10)$$

$$[M] = \frac{\rho A}{6}\frac{\Delta x}{\Delta t}\begin{pmatrix} 2 & 1 & -1 & -2 \\ 1 & 2 & -2 & -1 \\ -1 & -2 & 2 & 1 \\ -2 & -1 & 1 & 2 \end{pmatrix}. \quad (5.11)$$

From the elementary matrices, the global system of equations are constructed and following is the expression for the assembled matrix

$$[M-K]\{u\} + \left[\int_0^L \rho A\tilde{v}\frac{\partial \tilde{u}}{\partial t}dx\right]_{t=T} = \{f\} + \left[\int_0^L \rho A\tilde{v}\frac{\partial \tilde{u}}{\partial t}dx\right]_{t=0}. \quad (5.12)$$

The above system of equations is conditioned similar to that of (4.26), after which it is solved via a direct solve method to find the displacements. For details please refer to Appendix E.

5.3 Results

In this section the results obtained from the simulation are presented and the performance between the various methods are compared. The model properties are given in Table 5.1.

Tab 5.1 – Model properties for the axially vibrating bar

Category	**Value**
Elastic Modulus, E	200e+9Pa
Density, ρ	7870 kg/m^3
Cross Sectional Area, A	1 x 10^{-4} m^2
Bar Length, L	1 m
Time Span, T	0.0024 s
Initial Velocity magnitude, v_0	1 x 10^{-3} m/s
Initial Displacement magnitude, x_0	1 x 10^{-6} m

The response graph for the mass on spring model is given in Fig 5.4.

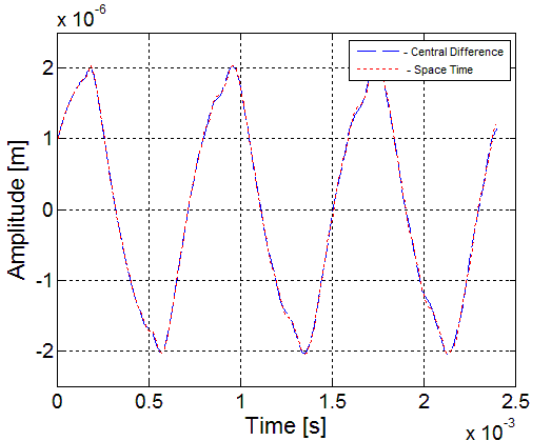

Figure 5.4 presents is the response graph at the tip of the axially vibrating bar for both the CD and STFEM methods using a Δx of 12 and Δt of 2400

The Central Difference approximation will act as the benchmark to which the 2D Space Time method is compared. As such, the CD solution must be checked for convergence. Convergence is found by comparing the relative change in tip displacement between two subsequent mesh densities and taking the median of the difference over the range of 2.5 x 10^{-3} seconds. Convergence is assumed when this error falls below 1%. The following figure shows results of the CD approach for a number of different Δx & Δt combinations.

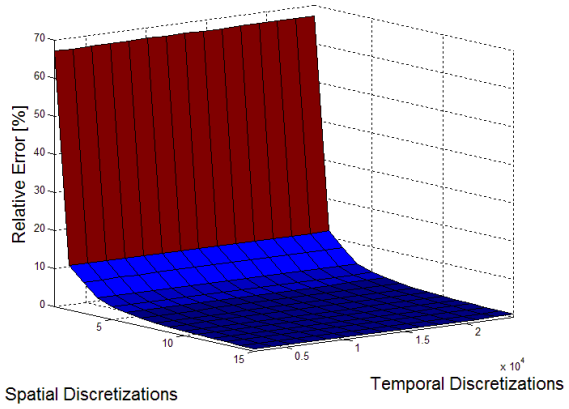

Fig 5.5- Relative error in the central difference model for various space-time mesh densities

An increase in the spatial mesh density results in significant decrease in relative error, while changing the temporal mesh density has comparatively less impact on the result.

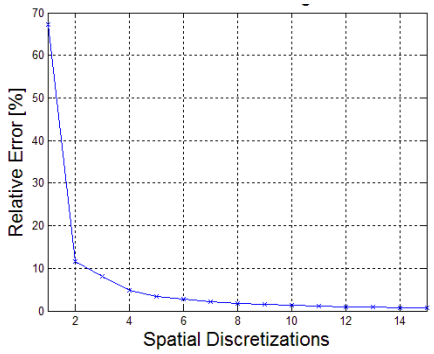

Fig 5.6- relative change of plot in error for increasing spatial discretizations at

$\Delta t = 2.4X10^{-6}\,s$ (*i.e.*, 1x10^4 temporal discretization)

In the above plot it can be noted that after 12 space elements the curve of the slope is below 1% change. Central Difference is a conditionally stable algorithm and is found to be stable for time step $\Delta t \le \left(2/\omega_{\max}\right)$ where $\omega_{\max}$ is the maximum natural frequency of the bar[16]. Note that the maximum natural frequency increases as the spatial density is increased. Based on the results from the Central Difference study, the solution is deemed to converged with 12 spatial discretizations and 2400 temporal discretizations.

Different mesh sizes are used to compare Space Time with the converged Central Difference solution. The relative error is found by comparing the tip displacement between the techniques: taking the median of the difference between the computed results for the Space-Time method for different mesh densities and the converged Central Difference solution. The convergence criteria is again a relative error of 1%.

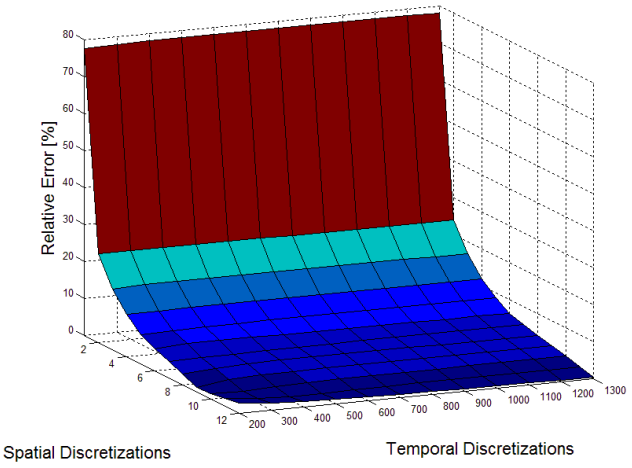

Fig 5.7- Convergence plot of central difference and space time methods

In figure 5.7 it can be noted that, similar to figure 5.5, an increase in spatial discretization results in significant change in the relative difference. Likewise an increase in temporal discretizations has relatively lesser effect on the computed displacement values.

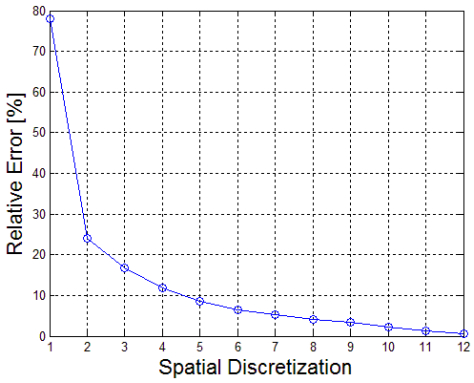

Fig 5.8 – Comparison between relative error for increasing spatial discretization at $\Delta t = 4.8X10^{-6}s$ (*i.e.*, 500 temporal elements)

At 12 spatial discretizations and 500 temporal discretizations, which result in $\Delta t = 4.8$e-6s, the Space-Time method converges to 1% relative error compared to the Central Difference solution. It is noticeable that the Space-Time method requires 5 times less time discretization to reach convergence compared to the Central Difference method.

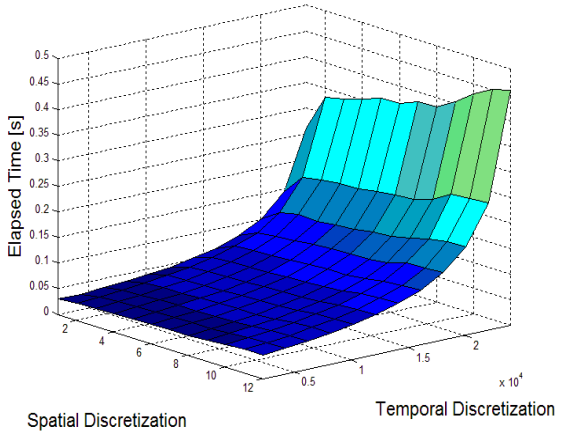

Fig 5.9 –Central Difference method's computation time for various mesh densities

Figure 5.9 shows the computational time against the number of discretizations in space and time. The 3D plot exhibits a curve with an increase in computational time as there is an increase in time and space dicretization, but the maximum time taken by Central Difference method is 0.5s, which is considerably less than the maximum time taken for the

space-time method. This could be attributed to the iterative solver used for the central difference method.

The following plot gives information on the computational expenditure for the space-time method.

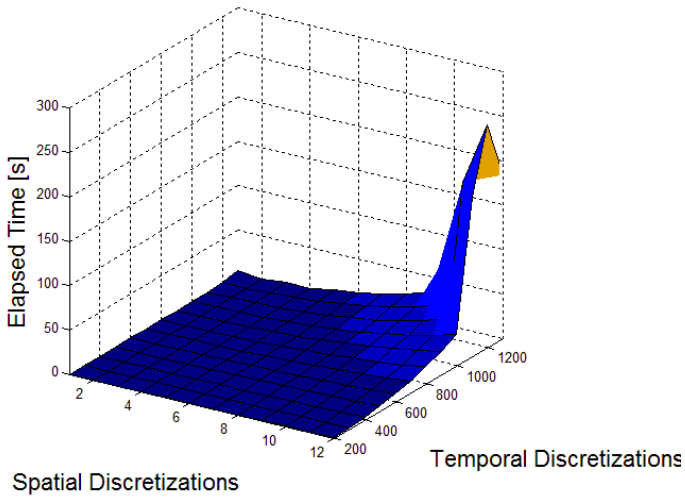

Fig 5.10 – 3D plot of the space-time method's computation time

Figure 5.10 shows that computation time required increases with a steep slope as the Space-Time mesh density increases.

5.4 Conclusion

The Space-Time and Central Difference methods require the same spatial discretizations to converge. It can also be noted that an increase in the number of temporal discretizations has comparatively little impact on the convergence result while an increase in space elements has a greater impact on the convergence result. While the computational time required for the Space-Time method generally increases with an increase in mesh density, the increase in computational time rises rapidly when the mesh density is beyond nine spatial discretizations and 1000 temporal discretizations. It is also noticeable that the value of time step for convergence of the Space-Time method is lesser than the time step required for the

Central Difference. But when comparing the total time required for both the methods to reach convergence it is noticeable that Space-Time requires 2 orders of magnitude more time than Central Differene and hence appears to be more computationally inefficient. It is hypothesized this finding is dependent on the solution algorithm so future work could shed light on computationally faster methods. For the present case and in the present form of implementation, the Central Difference approach is more computationally efficient than the space-time method for solving the dynamic response of an axially vibrating bar.

6. Conclusion

This comparative study between the Space-Time finite element method and the central difference method was explored and important attributes compared. The results offer a brief perspective into the performance of the STFEM in terms of accuracy and in terms of computational efficiency. In the case of mass-spring damper system, the Central Difference method is two orders of magnitude more accurate than TFEM linear while requiring only 6 x 10^{-3} s computationally whereas TFEM requires $2x10^{-1}$s to compute; quadratic elements yield accuracy to the order of 10^{-11} and is 6 orders more accurate than Central Difference but implementation of the technique in the present form requires 6 x 10^{0}s computational time which is three orders of magnitude more than Central Difference. In the case of the axially vibrating bar, the Central Difference method requires only 0.5s of computational time whereas the space-time method takes two orders of magnitude more time to compute, hence Central Difference is computationally less expensive. Again the reason could be the iterative solving of central difference method, which arguably takes less time than the method used for STFEM. A potential investigation could be made with an iterative implementation for STFEM. Our findings suggest that for the cases analysed and in the present form of our STFEM implementation, STFEM does not appear to have any significant advantage over classical finite difference methods.

Other future work could involve investigating mixed elements, where mixed elements would mean using elements with both continuous and discontinuous Galerkin formulation. Understanding efficiency characteristics of Space-Time implementation with unilateral and multilateral contact and higher order elements could also be of interest. For cases involving shock and discontinuities Space-Time in relation with eXtended Finite elements method (XFEM) could also be explored.

References

[1] - Fridtjov Irgens, "*Continuum Mechanics*", Springer Verlag, page 1-2 Print, 2007

[2] – Vladimir B. Poruchikov, "*Methods of the Classical Theory of Elastodynamics*", Springer Verlag, page 1-4 print, 1993

[3] – J.H.Argyris and D.W.Scharpf, "Finite Elements in Time And Space", *Nuclear Engineering and Design* 10 (1969) 456-464

[4] – Thomas.J.R.Hughes & Gregory M Hulbert, "Space-Time Finite Element Methods for Elastodynamics: Formulations and Error Estimates", *Computer Methods in Applied Mechanics and Engineering*, 66 (1988), 339-363 print.

[5] - Gregory M Hulbert & Thomas J.R. Hughes, "Space-Time Finite Element Methods for Second Order Hyperbolic Equation", *Computer Methods in Applied Mechanics and Engineering* 84 (1990), 327-348 print.

[6] - Donald A French, "A Space-Time Finite Element Method for the Wave Equation", *Computer Methods in Applied Mechanics and Engineering* 107 (1993) 145-157

[7] - X.D.Li, N.E.Wiberg, "Implementation and Adaptivity of a Space-Time Finite Element method for Structural Dynamics*", Computer Methods in Applied Mechanics and Engineering*, 156 (1998) 211-229.

[8] - Franck Jourdan, Serge Dumont, Tarik Madani. A Space-Time Finite Element Method for elastodynamics problems : elementary examples of 4D remeshing using simplex elements. 2013. <hal-01091356>

[9] - Matthew Anderson & Jung-Han Kimn, "A Numerical Approach to Space-Time Finite Elements for the Wave Equation", *Computer Physics*. (2007) 226:466-476,

[10] - S.Sathe, R.Benney, R.Charles, E.Doucette, J.Miletti, M.Senga, K.Stein, T.E.Tezduyar, "Fluid-Structure interaction modelling of complex parachute designs with the space-time finite element techniques", *Computers& Fluids* 36 (2007) 127-135

[11] – Tayfun E Tezduyar, Sunil Sathe, Ryan Keedy & Keith Stein,"Space–time finite element techniques for computation of fluid–structure interactions", *Computer Methods in Applied Mechanical Engineering* 195 (2006) 2002–2027

[12] – W.E.H. Sollie, O. Bokhove, J.J.W. van der Vegt, "Space–time discontinuous Galerkin finite element method for two-fluid flows", *Computational Physics* 230 (2011) 789–817

[13] - L.Karaoglan, A.K.Noor, "Space-time finite element methods for sensitivity analysis of contact/impact response of axisymmetric composite structures", *Computer Methods Application Mechanical Engineering*, Vol. 144 (1997) 371-389

[14] - O.C.Zeinkiewicz & R.L.Taylor, "*The Finite Element Method: The Basis*", fifth edition, Butterworth Heinemann, page 39-41, 58-61, print

[15] - Robert Cook *et al*, "*Concepts and Applications of Finite Element Analysis*", 4th edition, Wiley, page 193-198, print

[16] - Fish.J, Ted Belytschko, "*A First Course in Finite Elements*", Wiley, page 47-50, print 2007

[17] - S.S.Rao, "*The Finite Element Method in Engineering*", fifth edition, Butterworth Heinemann, page 99-105, print

[18] - Jonathan Baptista, "Space Time Finite Element Methods in Elastodynamics", McGill University, 2011

[19] – James F. Epperson, "*An Introduction to Numerical Methods and Analysis*", Wiley, 2nd Edition, page 193, print

[20] - Singiresu S. Rao, "*Vibration of Continuous Systems*", Wiley, print 2007

[21] – Cheng-Few Lee & Alice Lee, "*Encyclopaedia of Finance*" Springer Verlag, page – 102, print, 2006

Appendices

Appendix A

Analytical Solution for the 1D Forced Mass-Spring-Damper System.

From [20] the equation of motion for a forced, damped SDOF is

$$m\ddot{x} + c\dot{x} + kx = f_0 \sin(\omega t) \qquad \text{with } x(0) = x_0 \text{ and } \dot{x}(0) = v_0 \qquad \text{(A.1)}$$

where x is the displacement of the mass

t is the time variable

m is the mass

c is the damping coefficient

k is the stiffness

f_0 is the force amplitude

ω is the forcing frequency

x_0 is initial displacement

v_0 is initial velocity

The solution to this equation has two parts: the homogenous solution $x_h(t)$ and the particular solution $x_p(t)$. The homogenous solution satisfies the free vibration case and the particular satisfies the forced vibration case.

$$x_h(t) = e^{-\zeta\omega t}(C_1 \cos(\omega_d t) + C_2 \sin(\omega_d t)) \qquad \text{(A.2)}$$

$$x_p(t) = C_3 \cos(\omega t) + C_4 \sin(\omega t) \qquad \text{(A.3)}$$

C_1, C_2, C_3, C_4 are constants derived from the initial conditions

Natural frequency is found from $\omega_n = \sqrt{\frac{k}{m}}$ (A.4)

Damping ratio is found from $\zeta = \frac{c}{2m\omega_n}$ (A.5)

Damped natural frequency is found from $\omega_d = \omega_n\sqrt{1-\zeta^2}$ (A.6)

By substituting $x_p(t)$ and $x_h(t)$ into Eqn(A.1), it can be shown that:

$$C_3 = \frac{-f_0(\omega c)}{(k^2 - m\omega^2)^2 + (\omega c)^2} \tag{A.7}$$

$$C_4 = \frac{-f_0(k - m\omega^2)}{(k^2 - m\omega^2)^2 + (\omega c)^2} \tag{A.8}$$

$$C_1 = x_0 - C_3 \tag{A.9}$$

$$C_2 = \frac{v_0 + \zeta\omega_n C_1 - \omega C_4}{\omega_d} \tag{A.10}$$

Putting together the above values

$$x_T(t) = e^{-\zeta\omega_n t}\left(C_1\cos(\omega_d t) + C_2\sin(\omega_d t)\right) + C_3\cos(\omega t) + C_4\sin(\omega t) \tag{A.11}$$

Appendix B

Central Difference Formulation

The following section details the central difference formulation used for the mass-spring-damper problem [15].

The equation for the lumped mass vibration system in one dimension is given below.

$$m\ddot{q} + c\dot{q} + kq = f \tag{B.1}$$

where : m is the mass term

c is the damping term

k is the stiffness term

$\ddot{q}$ is the acceleration term

$\dot{q}$ is the velocity term

q is the displacement term

f is the forcing term

In Central Difference technique the velocity term is deduced from

$$\dot{q}_i = \frac{q_{i+1} - q_{i-1}}{2\Delta t} \tag{B.2}$$

and the acceleration term is deduced from

$$\ddot{q}_i = \frac{q_{i+1} - 2q_i + q_{i-1}}{\Delta t^2} \tag{B.3}$$

Substituting the above terms into equation (B.1)

$$m\left(\frac{q_{i+1}-2q_i+q_{i-1}}{\Delta t^2}\right)+c\left(\frac{q_{i+1}-q_{i-1}}{2\Delta t}\right)+kq_i=f_i \tag{B.4}$$

$$\Rightarrow \quad m\frac{q_{i+1}}{\Delta t^2}-m\frac{2q_i}{\Delta t^2}+m\frac{q_{i-1}}{\Delta t^2}+c\frac{q_{i+1}}{2\Delta t}-c\frac{q_{i-1}}{2\Delta t}+kq_i=f_i \tag{B.5}$$

$$\Rightarrow \quad m\frac{q_{i+1}}{\Delta t^2}+c\frac{q_{i+1}}{2\Delta t}-m\frac{2q_i}{\Delta t^2}+kq_i+m\frac{q_{i-1}}{\Delta t^2}-c\frac{q_{i-1}}{2\Delta t}=f_i \tag{B.6}$$

$$\Rightarrow \quad q_{i+1}\left(\frac{m}{\Delta t^2}+\frac{c}{2\Delta t}\right)+q_i\left(\frac{m}{\Delta t^2}+k\right)+q_{i-1}\left(\frac{m}{\Delta t^2}-\frac{c}{2\Delta t}\right)=f_i \tag{B.7}$$

$$\Rightarrow \quad q_{i+1}=\left(\frac{m}{\Delta t^2}+\frac{c}{2\Delta t}\right)^{-1}\left[f_i-q_i\left(\frac{m}{\Delta t^2}+k\right)-q_{i-1}\left(\frac{m}{\Delta t^2}-\frac{c}{2\Delta t}\right)\right] \tag{B.8}$$

The displacement at time interval $i+1$ is found using the Central Difference Technique as demonstrated in equation (B.8). From initial conditions the displacement and velocity at time t=0, which corresponds to *i*=2, can be found: $q_2=x_0$, $\dot{q}_2=v_0$. Substituting the values into equation (B.1) to find the acceleration at *i*=2 gives:

$$\ddot{q}_2=\frac{1}{m}\left(f_2-kq_2+c\dot{q}_2\right). \tag{B.9}$$

Displacement at *i*=1 is found from

$$q_1=q_2-\Delta t\dot{q}_2+\Delta t^2\frac{\ddot{q}_2}{2}. \tag{B.10}$$

Now that displacements at *i*=1 and *i*=2 are known, Eqn(B.8) can be iterated to find the remaining values. Displacement at third time step would be the following

$$q_3=\left(\frac{m}{\Delta t^2}+\frac{c}{2\Delta t}\right)^{-1}\left[f_i-q_2\left(\frac{m}{\Delta t^2}+k\right)-q_1\left(\frac{m}{\Delta t^2}-\frac{c}{2\Delta t}\right)\right]. \tag{B.11}$$

Appendix C

Linear Element Derivation for Finite Element in Time Formulation

The following section walks through the steps involved in developing the constituent element matrices used in Chapter 4. The constituent elements are found from the weak form of the single-degree-of-freedom equation of motion. Two element types were applied in Chapter 4, the linear element and the quadratic element. Appendix C deals with the development of the mass, stiffness, damping, boundary conditions and the forcing matrices for the linear element while Appendix D presents the development for the quadratic element.

The equation of motion is

$$m\ddot{x} + c\dot{x} + kx = f_0 \sin(\omega t). \tag{C.1}$$

Substituting the trial function $\tilde{u} = x$ provides,

$$m\ddot{\tilde{u}} + c\dot{\tilde{u}} + k\tilde{u} - f_0 \sin(\omega t) = Residual. \tag{C.2}$$

Applying the weak form of the equation

$$\int_0^T \tilde{v}\left(m\ddot{\tilde{u}} + c\dot{\tilde{u}} + k\tilde{u} - f_0 \sin(\omega t)\right)dt = 0. \tag{C.3}$$

Expanding the above equation

$$\int_0^T \tilde{v}\left(m\ddot{\tilde{u}}\right)dt + \int_0^T \tilde{v}\left(c\dot{\tilde{u}}\right)dt + \int_0^T \tilde{v}\left(k\tilde{u}\right)dt = \int_0^T \tilde{v}\left(f_0 \sin\left(\omega t\right)\right)dt. \tag{C.4}$$

Intergrating by parts

$$-\int_0^T \dot{\tilde{v}} m\dot{\tilde{u}}dt + \left[\tilde{v}m\dot{\tilde{u}}\right]_0^T + \int_0^T \tilde{v}\left(c\dot{\tilde{u}}\right)dt + \int_0^T \tilde{v}\left(k\tilde{u}\right)dt = \int_0^T \tilde{v}\left(f_0 \sin\left(\omega t\right)\right)dt. \tag{C.5}$$

The above equation is the developed weak form and each of the five terms can be developed into unique matrices.

First Term $-\int_0^T \dot{\tilde{v}} m \dot{\tilde{u}} dt$ develops into the mass matrix

Second Term $\left[\tilde{v} m \dot{\tilde{u}}\right]_0^T$ are the boundary conditions

Third Term $\int_0^T \tilde{v}\left(c\dot{\tilde{u}}\right) dt$ develops into the damping matrix

Fourth Term $\int_0^T \tilde{v}\left(k\tilde{u}\right) dt$ develops into the stiffness matrix

Fifth Term $\int_0^T \tilde{v}\left(f_0 \sin\left(\omega t\right)\right) dt$ develops into the forcing vector

The isoparametric linear element is explained in the Chapter 3. The shape functions of the linear element are

$$\left\{N\left(r\right)\right\} = \begin{Bmatrix} \frac{1-r}{2} \\ \frac{1+r}{2} \end{Bmatrix}. \qquad \text{(C.6)}$$

The trial function is

$$\tilde{u} = \left\{N(r)\right\}^T \left\{u_n\right\} = \begin{Bmatrix} \frac{1-r}{2} & \frac{1+r}{2} \end{Bmatrix} \begin{Bmatrix} u_1 \\ u_2 \end{Bmatrix}. \qquad \text{(C.7)}$$

The weighting function is

$$\tilde{v}_i = \frac{\partial \tilde{u}}{\partial u_i} \text{ for } i=1,2 \Rightarrow \tilde{v} = \left\{N(r)\right\} \qquad \text{(C.8)}$$

C.1 Mass Matrix

Substituting into the First Term and applying the chain rule while integrating over a typical element $[t_i, t_{i+1}]$

$$\int_{t_i}^{t_{i+1}} \frac{d\tilde{v}}{dr}\frac{dr}{dt} m \frac{d\tilde{u}}{dr}\frac{dr}{dt} dt \,. \tag{C.9}$$

The Mass Matrix is developed from the above equation, expanding it

$$\int_{t_i}^{t_{i+1}} \begin{Bmatrix} -1/2 \\ 1/2 \end{Bmatrix} \frac{dr}{dt} m \begin{Bmatrix} -1/2 & 1/2 \end{Bmatrix} \frac{dr}{dt} dt \begin{Bmatrix} u_i \\ u_{i+1} \end{Bmatrix},$$

(C.10)

$$\Rightarrow \qquad [M] = m \int_{t_i}^{t_{i+1}} \begin{bmatrix} \frac{1}{4} & \frac{-1}{4} \\ \frac{-1}{4} & \frac{1}{4} \end{bmatrix} \left(\frac{dr}{dt}\right)^2 dt \,. \tag{C.11}$$

Using the isoparametric approach to approximate the time variable, where t_i is the time at step *i* such that $t_{i+1} - t_i = \Delta t$

$$t(r) = \{N(r)\}^T \begin{Bmatrix} t_i \\ t_{i+1} \end{Bmatrix}. \tag{C.12}$$

Hence $\frac{dt}{dr}$ reduces to $\frac{\Delta t}{2}$; applying it in (C.11)

$$m \int_{t_i}^{t_{i+1}} \begin{bmatrix} \frac{1}{4} & \frac{-1}{4} \\ \frac{-1}{4} & \frac{1}{4} \end{bmatrix} \left(\frac{4}{\Delta t^2}\right) dt \,. \tag{C.13}$$

After integration, the mass matrix is obtained

$$[M] = \frac{m}{\Delta t} \begin{pmatrix} 1 & -1 \\ -1 & 1 \end{pmatrix}. \tag{C.14}$$

C.2 Boundary terms

Now considering the boundary condition term $\left[\tilde{v} m \dot{\tilde{u}}\right]_0^T$, where

$$\left[\tilde{v} m \dot{\tilde{u}}\right]_0^T = \left(\tilde{v} m \dot{\tilde{u}}\right)_T - \left(\tilde{v} m \dot{\tilde{u}}\right)_0 . \tag{C.15}$$

In the above equation, consider the term $\left(\tilde{v}m\dot{\tilde{u}}\right)_0$. The value of $\dot{\tilde{u}}$ at 0 is known from the initial velocity v_0, hence the term reduces to $mv_0\begin{Bmatrix}\frac{1-r}{2}\\ \frac{1+r}{2}\end{Bmatrix}_{t=0}$. From the isoparametric limits of integration of [-1,1], at time step *t=0*, the value of *r* is -1 on the first element and is substituted to obtain the boundary condition vector $mv_0\begin{Bmatrix}1\\0\end{Bmatrix}$.

The $[\tilde{v}m\dot{\tilde{u}}]_T$ term is considered. At time step t=T, the value of r is +1 for the last element

$$\left[\tilde{v}m\dot{\tilde{u}}\right]_{t=T} = \tilde{v}m\left.\frac{d\dot{\tilde{u}}}{dt}\right|_{t=T},$$

$$\Rightarrow \qquad \left.\tilde{v}m\frac{d\dot{\tilde{u}}}{dt}\right|_{t=T} = \left.\tilde{v}m\frac{d\dot{\tilde{u}}}{dr}\frac{dr}{dt}\right|_{t=T}. \qquad \text{(C.17)}$$

Time step $t = T$ equates to the right side of the final element (*i.e.*, *r* = 1) and is substituted in equation (C.17)

$$\Rightarrow \qquad \begin{Bmatrix}\frac{1-r}{2}\\ \frac{1+r}{2}\end{Bmatrix} m\begin{Bmatrix}-1/2 & 1/2\end{Bmatrix}\left.\frac{2}{\Delta t}\right|_{r=1}\begin{Bmatrix}u_{i-1}\\ u_i\end{Bmatrix}. \qquad \text{(C.18)}$$

After simplification, the boundary condition matrix is obtained

$$\frac{m}{\Delta t}\begin{bmatrix}0 & 0\\ -1 & 1\end{bmatrix}\begin{Bmatrix}u_{i-1}\\ u_i\end{Bmatrix}. \qquad \text{(C.19)}$$

The above boundary condition is found at the final time step *T*, hence it is added to rows and columns of $n-1$ and n the assembled matrix.

C.3 Damping matrix

Now considering the damping matrix.

$$\int_{t_n}^{t_{n+1}} \tilde{v}\left(c\dot{\tilde{u}}\right)dt\ , \qquad \text{(C.20)}$$

$$\Rightarrow \qquad \int_{t_i}^{t_{i+1}} \begin{Bmatrix}\frac{1-r}{2}\\ \frac{1+r}{2}\end{Bmatrix} c\begin{Bmatrix}\frac{1}{2} & \frac{1}{2}\end{Bmatrix}\frac{dr}{dt}dt\begin{Bmatrix}u_i\\ u_{i+1}\end{Bmatrix}, \qquad \text{(C.21)}$$

$$\Rightarrow \qquad [C]=\int_{-1}^{1}\begin{Bmatrix}\frac{1-r}{2}\\ \frac{1+r}{2}\end{Bmatrix} c\begin{Bmatrix}\frac{1}{2} & \frac{1}{2}\end{Bmatrix}\frac{dr}{dt}\frac{dt}{dr}dr\,. \tag{C.22}$$

After integrating, the damping matrix is obtained

$$[C]=\frac{c}{2}\begin{bmatrix}-1 & 1\\ -1 & 1\end{bmatrix}. \tag{C.23}$$

C.4 Stiffness matrix

Now considering the Stiffness Matrix

$$\int_{t_i}^{t_{i+1}} \tilde{v}k\tilde{u}dt\,, \tag{C.24}$$

$$\Rightarrow \qquad \int_{-1}^{1}\begin{Bmatrix}\frac{1-r}{2}\\ \frac{1+r}{2}\end{Bmatrix} k\begin{Bmatrix}\frac{1-r}{2} & \frac{1+r}{2}\end{Bmatrix}\frac{dt}{dr}dr\begin{Bmatrix}u_i\\ u_{i+1}\end{Bmatrix}, \tag{C.25}$$

$$\Rightarrow \qquad [K]=k\int_{-1}^{1}\begin{Bmatrix}\frac{(1-r)^2}{4} & \frac{1-r^2}{4}\\ \frac{1-r^2}{4} & \frac{(1+r)^2}{4}\end{Bmatrix}\frac{\Delta t}{2}dr\,. \tag{C.26}$$

Integrating and further simplifying the above equation, the stiffness matrix is obtained

$$[K]=\frac{k\Delta t}{6}\begin{bmatrix}2 & 1\\ 1 & 2\end{bmatrix}. \tag{C.27}$$

C.5 Force vector

Now considering the forcing term $\int_{t_i}^{t_{i+1}} \tilde{v}\left(f_0\sin(\omega t)\right)dt$

Using the linear shape functions in the time domain instead of the linear isoparametric shape functions.

$$\begin{Bmatrix}\frac{t_{i+1}-t}{t_{i+1}-t_i}\\ \frac{t-t_i}{t_{i+1}-t_i}\end{Bmatrix} \tag{C.28}$$

Linear shape functions in the time domain are considered for ease of substitution of limits and calculation.

$$\int_{t_i}^{t_{i+1}} \begin{Bmatrix} \dfrac{t_{i+1}-t}{t_{i+1}-t_i} \\ \dfrac{t-t_i}{t_{i+1}-t_i} \end{Bmatrix} \left(f_0 \sin\left(\omega t\right)\right) dt \,, \tag{C.29}$$

$$\Rightarrow \quad \frac{f_0}{\Delta t} \int_{t_i}^{t_{i+1}} \begin{Bmatrix} t_{i+1}-t \\ t-t_i \end{Bmatrix} \left(\sin\left(\omega t\right)\right) dt \,. \tag{C.30}$$

After integration

$$\begin{Bmatrix} \dfrac{f_0\left(\sin(t_i\omega)-\sin(t_{i+1}\omega)-t_n\omega\cos(t_i\omega)+t_{i+1}\omega\cos(t_i\omega)\right)}{\Delta t\omega^2} \\ \dfrac{-f_0\left(\sin(t_i\omega)-\sin(t_{i+1}\omega)-t_n\omega\cos(t_{i+1}\omega)+t_{i+1}\omega\cos(t_{i+1}\omega)\right)}{\Delta t\omega^2} \end{Bmatrix}. \tag{C.31}$$

Appendix D

Quadratic Element Derivation for Single Degree of Freedom Space-Time Finite Element Formulation

The nature of the isoparametric quadratic element is explained in the Chapter 3. The isoparametric shape functions for the quadratic elements are.

$$\left\{N\left(r\right)\right\}=\begin{Bmatrix}\dfrac{-r(1-r)}{2}\\ 1-r^2\\ \dfrac{r(1+r)}{2}\end{Bmatrix}. \qquad \text{(D.1)}$$

The trial function

$$\tilde{u}=\begin{Bmatrix}\dfrac{-r(1-r)}{2} & 1-r^2 & \dfrac{r(1+r)}{2}\end{Bmatrix}\left\{u_n\right\}. \qquad \text{(D.2)}$$

The weighting function

$$\tilde{v}=\begin{Bmatrix}\dfrac{-r(1-r)}{2}\\ 1-r^2\\ \dfrac{r(1+r)}{2}\end{Bmatrix}. \qquad \text{(D.3)}$$

D.1 Mass matrix

Applying the isoparametric transformation on the First Term from $\int_0^L \tilde{v}\left[\frac{d}{dx}\left(AE\frac{d\tilde{u}}{dx}\right)\right]dx=0$ for a typical element

$$\int_{t_{i-1}}^{t_{i+1}}\left(\frac{d\tilde{v}}{dt}m\frac{d\tilde{u}}{dt}\right)dt, \qquad \text{(D.4)}$$

$$\Rightarrow \qquad \int_{-1}^{1}\left(\frac{d\tilde{v}}{dr}\frac{dr}{dt}m\frac{d\tilde{u}}{dr}\frac{dr}{dt}\right)\frac{dt}{dr}dr, \qquad \text{(D.5)}$$

$$\Rightarrow \qquad \int_{-1}^{1}\left(\begin{Bmatrix} r-\frac{1}{2} \\ -2r \\ r+\frac{1}{2} \end{Bmatrix} m \begin{Bmatrix} r-\frac{1}{2} \\ -2r \\ r+\frac{1}{2} \end{Bmatrix}^{T} \left(\frac{dr}{dt}\right)^{2}\right)\frac{dt}{dr}\,dr \begin{Bmatrix} u_{i-1} \\ u_i \\ u_{i+1} \end{Bmatrix}. \qquad \text{(D.6)}$$

The transform between the time and the isoparametric coordinate is expressed using

$$\{t(r)\} = \{N(r)\}^{T} \begin{Bmatrix} t_{i-1} \\ t_i \\ t_{i+1} \end{Bmatrix}, \qquad \text{(D.7)}$$

After expanding and simplifying (D.7) reduces to

$$\{t(r)\} = (t_i + \Delta t r). \qquad \text{(D.8)}$$

The transform for *dt/dr* is expressed using

$$\frac{d\{t(r)\}}{dr} = \frac{d}{dr}\left(\{N(r)\}^{T} \begin{Bmatrix} t_{i-1} \\ t_i \\ t_{i+1} \end{Bmatrix}\right), \qquad \text{(D.10)}$$

$$\Rightarrow \qquad \frac{d\{t(r)\}}{dr} = \left\{t_{i+1}(r+\frac{1}{2}) - 2rt_i - t_{i-1}(r-\frac{1}{2})\right\}.$$

(D.11)

Substituting (D.8) in equation (D.6)

$$\int_{-1}^{1}\left(\begin{Bmatrix} r-\frac{1}{2} \\ -2r \\ r+\frac{1}{2} \end{Bmatrix} m \begin{Bmatrix} r-\frac{1}{2} \\ -2r \\ r+\frac{1}{2} \end{Bmatrix}^{T}\right)\frac{1}{\left\{t_{i+1}(r+\frac{1}{2}) - 2rt_i - t_{i-1}(r-\frac{1}{2})\right\}}\,dr \begin{Bmatrix} u_{i-1} \\ u_i \\ u_{i+1} \end{Bmatrix}. \qquad \text{(D.12)}$$

After integration, the mass matrix is obtained

$$[M] = \frac{m}{6\Delta t}\begin{pmatrix} 7 & -8 & 1 \\ -8 & 16 & -8 \\ 1 & -8 & 7 \end{pmatrix}.$$

(D.13)

D.2 Boundary terms

Now considering Boundary Condition $\left[\tilde{v}m\dot{\tilde{u}}\right]_0^T$

$$\left[\tilde{v}m\dot{\tilde{u}}\right]_0^T = \left(\tilde{v}m\dot{\tilde{u}}\right)_T - \left(\tilde{v}m\dot{\tilde{u}}\right)_0 . \tag{D.14}$$

The term $\left(\tilde{v}m\dot{\tilde{u}}\right)_0$ reduces to $mv_0 \left\{ \begin{array}{c} \frac{-r(1-r)}{2} \\ 1-r^2 \\ \frac{r(1+r)}{2} \end{array} \right\}\Bigg|_{t=0}$ with the weighting function having the

quadratic shape functions and as applied in Appendix C, at the first time step t = 0 the value

of r = -1 is substituted to obtain the boundary condition vector $mv_0 \left\{ \begin{array}{c} 1 \\ 0 \\ 0 \end{array} \right\}$ for the first element.

Now considering the term $\left(\tilde{v}m\dot{\tilde{u}}\right)_T$

$$\left(\tilde{v}m\dot{\tilde{u}}\right)_T = \tilde{v}m\frac{d\tilde{u}}{dt}\Bigg|_T \tag{D.15}$$

$$\Rightarrow \quad m\left\{ \begin{array}{c} \frac{-r(1-r)}{2} \\ 1-r^2 \\ \frac{r(1+r)}{2} \end{array} \right\}\left\{ r-\frac{1}{2} \quad -2r \quad r+\frac{1}{2} \right\}\Bigg|_T \left\{ \begin{array}{c} u_{n-2} \\ u_{n-1} \\ u_n \end{array} \right\}. \tag{D.16}$$

After substituting r = 1 in place of T, the boundary condition matrix is obtained

$$\frac{m}{\Delta t}\begin{bmatrix} 0 & 0 & 0 \\ 0 & 0 & 0 \\ 1 & -4 & 3 \end{bmatrix}\left\{ \begin{array}{c} u_{n-2} \\ u_{n-1} \\ u_n \end{array} \right\}. \tag{D.17}$$

Now considering the damping term $\int_0^T \tilde{v}c\left(\dot{\tilde{u}}\right)dt$

$$\Rightarrow \qquad c\int_{-1}^{1}\tilde{v}\left(\frac{d\tilde{v}^T}{dr}\frac{dr}{dt}\right)\frac{dt}{dr}dr\,, \tag{D.18}$$

$$\Rightarrow \qquad c\int_{-1}^{1}\begin{Bmatrix}\frac{-r(1-r)}{2}\\ 1-r^2\\ \frac{r(1+r)}{2}\end{Bmatrix}\begin{Bmatrix}r-\frac{1}{2}\\ -2r\\ r+\frac{1}{2}\end{Bmatrix}^T dr\begin{Bmatrix}u_{i-1}\\ u_i\\ u_{i+1}\end{Bmatrix}. \tag{D.19}$$

After Integration, the damping matrix is obtained

$$\Rightarrow \qquad [C]=\frac{c}{6}\begin{bmatrix}-3 & 4 & -1\\ -4 & 0 & 4\\ 1 & -4 & 3\end{bmatrix}. \tag{D.20}$$

D.4 Stiffness matrix

Now considering the Stiffness Term $\int_0^T \tilde{v}k\left(\tilde{u}\right)dt$

$$\Rightarrow \qquad k\int_{-1}^{1}\begin{Bmatrix}\frac{-r(1-r)}{2}\\ 1-r^2\\ \frac{r(1+r)}{2}\end{Bmatrix}\begin{Bmatrix}\frac{-r(1-r)}{2}\\ 1-r^2\\ \frac{r(1+r)}{2}\end{Bmatrix}^T \frac{dt}{dr}dr\begin{Bmatrix}u_{i-1}\\ u_i\\ u_{i+1}\end{Bmatrix}. \tag{D.21}$$

$$\Rightarrow k\int_{-1}^{1}\begin{Bmatrix}\frac{-r(1-r)}{2}\\ 1-r^2\\ \frac{r(1+r)}{2}\end{Bmatrix}\begin{Bmatrix}\frac{-r(1-r)}{2}\\ 1-r^2\\ \frac{r(1+r)}{2}\end{Bmatrix}^T \left\{t_{n-1}(r-\frac{1}{2})-2rt_n+t_{n+1}(r+\frac{1}{2})\right\}dr\begin{Bmatrix}u_{i-1}\\ u_i\\ u_{i-1}\end{Bmatrix}. \tag{D.22}$$

After Integration the Stiffness Matrix is obtained

$$[K]=\frac{k\Delta t}{15}\begin{bmatrix}4 & 2 & -1\\ 2 & 16 & 2\\ -1 & 2 & 4\end{bmatrix}. \qquad \text{(D.23)}$$

D.5 Force vector

Now considering the forcing term $\int_0^T \tilde{v} f_0 \sin(\omega t)dt$ and substituting (D.9) in the forcing term in place of *t* and expanding the term

$$\Rightarrow \quad \int_{-1}^{1}\begin{Bmatrix}\frac{-r(1-r)}{2}\\ 1-r^2\\ \frac{r(1+r)}{2}\end{Bmatrix} f_0 \sin\left(\omega\left(t_i+\Delta t r\right)\right)\frac{dt}{dr}dr\,. \qquad \text{(D.24)}$$

After integration

$$\begin{Bmatrix}\frac{\Delta t f_0}{2}\left(\frac{\left(4\cos(\Delta t\omega)\sin(t_i\omega)\right)}{\Delta t^2\omega^2}+\frac{2\sin(\Delta t\omega)\sin(t_i\omega)}{\Delta t\omega}-\frac{4\sin(\Delta t\omega)\sin(t_i\omega)}{\Delta t^3\omega^3}\right)-\frac{f_0\cos(t_i\omega)\left(\sin(\Delta t\omega)-\Delta t\omega\cos(\Delta t\omega)\right)}{\Delta t\omega^2}\\ \frac{4f_0\sin(\Delta t\omega)\sin(t_i\omega)}{\Delta t^2\omega^3}-\frac{4f_0\cos(\Delta t\omega)\sin(t_i\omega)}{\Delta t\omega^2}\\ \frac{\Delta t f_0}{2}\left(\frac{\left(4\cos(\Delta t\omega)\sin(t_i\omega)\right)}{\Delta t^2\omega^2}+\frac{2\sin(\Delta t\omega)\sin(t_i\omega)}{\Delta t\omega}-\frac{4\sin(\Delta t\omega)\sin(t_i\omega)}{\Delta t^3\omega^3}\right)+\frac{f_0\cos(t_i\omega)\left(\sin(\Delta t\omega)-\Delta t\omega\cos(\Delta t\omega)\right)}{\Delta t\omega^2}\end{Bmatrix}$$

where Δt is the time step.

Appendix E

Bilinear Quadrilateral Element Derivation for Axially Vibrating Bar in Space-Time Finite Element Formulation

In this section, the element matrices used in Chapter 5 are derived. The governing equation of motion for a bar is as follows.

$$EA\frac{\partial^2 u}{\partial x^2} - \rho A\frac{\partial^2 u}{\partial t^2} + f = 0. \tag{E.1}$$

where, E is the young's modulus

A is the area

ρ is the density

u is displacement as a function of space 'x' and time 't': $u(x,t)$

f is body load acting on the bar: $f(x,t)$

For the present case, body load is considered negligible. After applying the weak form the above equation reduces to the constituent elementary matrices.

$$\int_0^T\int_0^L \tilde{v}\left(EA\frac{\partial^2 \tilde{u}}{\partial x^2} - \rho A\frac{\partial^2 \tilde{u}}{\partial t^2}\right)dxdt = 0. \tag{E.2}$$

$$\int_0^T\int_0^L \tilde{v}EA\frac{\partial^2 \tilde{u}}{\partial x^2}dxdt - \int_0^T\int_0^L \tilde{v}\rho A\frac{\partial^2 \tilde{u}}{\partial t^2}dxdt = 0. \tag{E.3}$$

Expanding equation (E.3) using two integration by parts

$$-\int_0^T\int_0^L EA\frac{\partial \tilde{v}}{\partial x}\frac{\partial \tilde{u}}{\partial x}dxdt + \left[\int_0^T \tilde{v}EA\frac{\partial \tilde{u}}{\partial x}\right]_0^L - \left(-\int_0^T\int_0^L \rho A\frac{\partial \tilde{v}}{\partial t}\frac{\partial \tilde{u}}{\partial t}dxdt + \left[\int_0^L \tilde{v}\rho A\frac{\partial \tilde{u}}{\partial t}dxdt\right]_0^T\right) = 0. \tag{E.4}$$

From the above equation the constituent terms for stiffness, mass, forcing and boundary conditions are obtained. The following would be the term to derive for the stiffness matrix,

$$\int_0^T \int_0^L EA \frac{\partial \tilde{v}}{\partial x} \frac{\partial \tilde{u}}{\partial x} dx dt \,. \tag{E.5}$$

Two dimensional discretization is done using bilinear quadrilateral elements as explained in the Chapter 3. The following is the shape function used:

$$N = \begin{Bmatrix} \frac{1}{4}(1+\eta)(1+\xi) \\ \frac{1}{4}(1-\eta)(1+\xi) \\ \frac{1}{4}(1-\eta)(1-\xi) \\ \frac{1}{4}(1+\eta)(1-\xi) \end{Bmatrix}. \tag{E.6}$$

In the above equation space domain is mapped to 'η' and time domain is mapped to'ξ' .

Using the chain rule the local coordinates of bilinear quadrilateral are applied to (E.5)

$$\int_{-1}^{1} \int_{-1}^{1} [B]^T EA[B] \left| [J] \right| d\eta d\xi \,. \tag{E.7}$$

$$\text{Where} [B] = \begin{bmatrix} \frac{\partial N_1}{\partial S} & \frac{\partial N_2}{\partial S} & \frac{\partial N_3}{\partial S} & \frac{\partial N_4}{\partial S} \\ \frac{\partial N_1}{\partial T} & \frac{\partial N_2}{\partial T} & \frac{\partial N_3}{\partial T} & \frac{\partial N_4}{\partial T} \end{bmatrix} \text{ and } [J] = \begin{bmatrix} \frac{\partial S}{\partial \eta} & \frac{\partial T}{\partial \eta} \\ \frac{\partial S}{\partial \xi} & \frac{\partial T}{\partial \xi} \end{bmatrix} \tag{E.8}$$

After integration, the element stiffness matrix is obtained.

$$[K] = \frac{EA}{6} \frac{\Delta t}{\Delta x} \begin{pmatrix} 2 & -2 & -1 & 1 \\ -2 & 2 & 1 & -1 \\ -1 & 1 & 2 & -2 \\ 1 & -1 & -2 & 2 \end{pmatrix}. \tag{E.9}$$

The following is the derivation for the mass element matrix:

$$\int_0^T \int_0^L \rho A \frac{\partial \tilde{v}}{\partial t} \frac{\partial \tilde{u}}{\partial t} dx dt . \qquad \text{(E.10)}$$

From the above equation, applying the local coordinate transformation produces

$$\int_{-1}^{1} \int_{-1}^{1} [B]^T \rho A [B] \left| [J] \right| d\eta d\xi . \qquad \text{(E.11)}$$

After integration, the element mass matrix is obtained.

$$[M] = \frac{\rho A}{6} \frac{\Delta x}{\Delta t} \begin{pmatrix} 2 & 1 & -1 & -2 \\ 1 & 2 & -2 & -1 \\ -1 & -2 & 2 & 1 \\ -2 & -1 & 1 & 2 \end{pmatrix}. \qquad \text{(E.12)}$$

Temporal Boundary Conditions (TBC) = $\left[\int_0^L \rho A \tilde{v} \frac{\partial \tilde{u}}{\partial t} dx \right]_{t=0}$, $\left[\int_0^L \rho A \tilde{v} \frac{\partial \tilde{u}}{\partial t} dx \right]_{t=T}$,

Spatial Boundary Conditions (SBC) = $\left[\int_0^T EA \tilde{v} \frac{\partial \tilde{u}}{\partial x} dt \right]_{x=0}$, $\left[\int_0^T EA \tilde{v} \frac{\partial \tilde{u}}{\partial x} dt \right]_{x=L}$. (5.6)

Treatment of spatial boundary conditions are explained in section 5.3. In this section temporal boundary conditions are given a closer consideration. Consider the following term:

$$\left[\int_0^L \rho A \frac{\partial \tilde{u}}{\partial t} \tilde{v} dx \right]_{t=0} . \qquad \text{(E.21)}$$

Performing change of a variable for a typical element: $\left[\int_{-1}^{1} \rho A \frac{\partial \tilde{u}}{\partial t} \tilde{v} \frac{dx}{dr} dr \right]_{t=0}$. (E.22)

At $t = 0$, $\frac{\partial \tilde{u}}{\partial t} = v_0$

$$\left[\int_{-1}^{1} \rho A v_0 \tilde{v} \frac{dx}{dr} dr\right]_{t=0} \tag{E.23}$$

$$\int_{-1}^{1} \rho A v_0 \begin{Bmatrix} \frac{(1-r)}{2} \\ \frac{(1+r)}{2} \end{Bmatrix} \frac{dx}{dr} dr \tag{E.24}$$

$$\int_{-1}^{1} \rho A v_0 \begin{Bmatrix} \frac{(1-r)}{2} \\ \frac{(1+r)}{2} \end{Bmatrix} \frac{\Delta x}{2} dr \tag{E.25}$$

After integration, the boundary condition vector is obtained.

$$\frac{\rho A v_0 \Delta x}{2} \begin{bmatrix} 1 \\ 1 \end{bmatrix}. \tag{E.26}$$

The above vector is added to the forcing condition at nodes 1 through 7, using the direct assembly approach. The nodal positions at the end of the bar which are attached to the wall, (*i.e.*, 1,8,15,22,29) are constrained and the corresponding rows and columns are eliminated. Figure E.1 depicts the nodal locations for clarity.

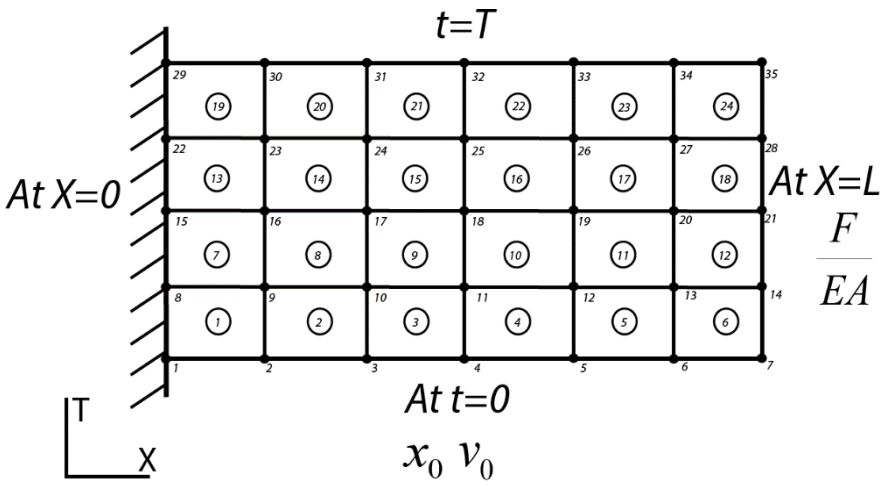

Fig E.1 – Nodal and Element locations on the discretized bar.

To accommodate the initial displacement, new rows containing zeros are introduced into the assembled matrix and the forcing vector similar to the SDOF approach. Initial displacement is applied using the formula $x_0 \sin\left(\frac{\pi x_i}{2l}\right)$ and is added to the bottom of the forcing vector to enforce the condition. On the side of the assembled matrix, ones are added along the diagonal cells to have the effect of making the displacement values at nodes 1 through 7 to be equal to the corresponding values of the forcing vector.

Due to the introduction of the new rows, the assembled matrix becomes rectangular matrix. The rows associated with the t=T nodes are chosen (i.e., 29 through 35 in this example) to be eliminated. Hence 6 rows are arbitrarily eliminated to regain the square shape. Now, the system of equations have all the boundary and initial conditions accommodated and is ready to be solved.